

# The $NN \rightarrow N\Delta$ cross section in nuclear matter\*

A.B. Larionov<sup>†</sup> and U. Mosel

*Institut für Theoretische Physik, Universität Giessen, D-35392 Giessen, Germany*

(Dated: November 12, 2018)

## Abstract

We present calculations of the  $NN \rightarrow N\Delta$  cross section in nuclear matter within the one-pion exchange model taking into account pion collectivity, vertex renormalization by the contact nuclear interactions and Dirac effective masses of the baryons due to coupling with the scalar  $\sigma$  field. Introducing the Dirac effective masses leads to an in-medium reduction of the cross section. The experimental data on pion multiplicities from the collisions of Ca+Ca, Ru+Ru and Au+Au at  $0.4 \div 1.5$  A GeV are well described by BUU calculations with the in-medium cross section.

PACS numbers: 25.75.Dw; 21.65.+f; 25.75.-q; 24.10.Jv

Keywords:  $NN \rightarrow N\Delta$  cross section; OPEM; baryon effective mass; BUU; C+C, Ca+Ca, Ru+Ru, Au+Au at  $0.4 \div 2$  A GeV; pion production

---

\* Supported by BMBF and GSI Darmstadt

<sup>†</sup> On leave from RRC "I.V. Kurchatov Institute", 123182 Moscow, Russia

## I. INTRODUCTION

While transport calculations have, in general, been very successful in describing particle production in heavy-ion collisions [1, 2, 3, 4, 5, 6, 7, 8, 9, 10, 11], one of the remaining open problems in the transport-theoretical description of heavy-ion collisions at SIS energies ( $\sim 1$  A GeV) is an overprediction of the pion multiplicity [5, 7, 8, 9, 12, 13]. At the beam energies of a few A GeV the dominating mechanism of the pion production is the excitation of the  $\Delta(1232)$  resonance in a nucleon-nucleon (NN) collision followed by its decay:  $NN \rightarrow N\Delta$ ,  $\Delta \rightarrow N\pi$ . The pion multiplicity, therefore, depends crucially on the value of the in-medium  $NN \rightarrow N\Delta$  cross section which – by detailed balance – also determines the pion reabsorption. In Ref. [13] a phenomenological density-dependent modification factor of the vacuum  $NN \rightarrow N\Delta$  cross section has been proposed. The BUU calculations with the density dependent  $NN \leftrightarrow N\Delta$  cross sections are in a reasonable agreement with the experimental data on pion production [13].

The purpose of the present work is to get rid of the ad-hoc description of Ref. [13] and to calculate the in-medium  $NN \leftrightarrow N\Delta$  cross sections on the basis of the one-pion exchange model (OPEM) with medium modifications. The calculated cross sections are used then in the BUU model to study the pion production in heavy-ion collisions at SIS energies.

It has been shown in Ref. [14] within the relativistic Dirac-Brueckner approach that the  $NN \rightarrow N\Delta$  cross section is reduced at high densities. Later studies within the OPEM including pion collectivity and vertex corrections [15, 16, 17] have shown, however, that the  $NN \rightarrow N\Delta$  cross section grows with nuclear density. An important contribution which was missed in Refs. [15, 16, 17] is given by the Dirac effective nucleon and  $\Delta$  resonance masses. We will show, that the introduction of the Dirac effective nucleon and  $\Delta$  masses in the OPEM leads to an in-medium reduction of the  $NN \leftrightarrow N\Delta$  cross sections in agreement with Ref. [14].

The structure of the paper is as follows: In Sect. II we describe the OPEM with medium modifications including pion collectivity, vertex renormalization by the contact interactions and effective masses for the nucleon and  $\Delta$  resonance. The energy dependence of the total  $pp \rightarrow n\Delta^{++}$  cross section as well as the angular and  $\Delta$  resonance mass dependencies of the differential  $pp \rightarrow n\Delta^{++}$  cross section are studied at finite nuclear matter densities. Sect. III explains how the in-medium modified cross sections are implemented into the BUU code and

describes the results of the BUU calculations of pion production from heavy-ion collisions at  $0.5 \div 2$  A GeV. In sect. IV the summary of our results and of remaining problems is given.

## II. THE MODEL

For the calculation of the  $NN \rightarrow N\Delta$  cross section in nuclear matter we apply the nonrelativistic OPEM similar to Ref. [15], however, with readjusted parameters. We have chosen the nonrelativistic version since it incorporates the contact nuclear interactions in a natural way, which is necessary in the in-medium calculations.

In the nonrelativistic reduction (c.f. Ref. [18]) the  $\pi NN$  and  $\pi N\Delta$  interaction Lagrangians are:

$$\mathcal{L}_{\pi NN} = \frac{f}{m_\pi} \psi^\dagger \sigma_\alpha \boldsymbol{\tau} \psi \nabla_\alpha \boldsymbol{\pi} , \quad (1)$$

$$\mathcal{L}_{\pi N\Delta} = \frac{f_\Delta}{m_\pi} \psi_\Delta^\dagger S_\alpha \mathbf{T} \psi \nabla_\alpha \boldsymbol{\pi} + h.c. , \quad (2)$$

where  $\psi$ ,  $\psi_\Delta$  and  $\boldsymbol{\pi}$  are the nucleon,  $\Delta$  resonance and pion field respectively.  $f = 1.008$  and  $f_\Delta = 2.202$  are the coupling constants [19].  $\sigma_\alpha$  and  $\boldsymbol{\tau}$  are the spin and isospin Pauli matrices.  $S_\alpha$  and  $\mathbf{T}$  are the spin and isospin transition ( $1/2 \rightarrow 3/2$ ) operators defined according to Ref. [20].

The nuclear spin-isospin short range correlations are known to be important for the in-medium  $NN \rightarrow N\Delta$  cross section [15]. We will introduce them via the following Lagrangian:

$$\begin{aligned} \mathcal{L}_{SRC} = & -\frac{f^2}{2m_\pi^2} g'_{NN} (\psi^\dagger \sigma_\alpha \boldsymbol{\tau} \psi) (\psi^\dagger \sigma_\alpha \boldsymbol{\tau} \psi) \\ & - \left[ \frac{f f_\Delta}{m_\pi^2} g'_{N\Delta} (\psi^\dagger \sigma_\alpha \boldsymbol{\tau} \psi) (\psi_\Delta^\dagger S_\alpha \mathbf{T} \psi) + h.c. \right] \\ & -\frac{f_\Delta^2}{m_\pi^2} g'_{\Delta\Delta} (\psi_\Delta^\dagger S_\alpha \mathbf{T} \psi) (\psi_\Delta^\dagger S_\alpha^\dagger \mathbf{T}^\dagger \psi_\Delta) \\ & - \left[ \frac{f_\Delta^2}{2m_\pi^2} g'_{\Delta\Delta} (\psi_\Delta^\dagger S_\alpha \mathbf{T} \psi) (\psi_\Delta^\dagger S_\alpha \mathbf{T} \psi) + h.c. \right] \end{aligned} \quad (3)$$

$g'_{NN}$ ,  $g'_{N\Delta}$  and  $g'_{\Delta\Delta}$  are the Landau-Migdal parameters.

The values of the Landau-Migdal parameters are not fixed unambiguously in the literature. Within a simple universality assumption  $g'_{NN} = g'_{N\Delta} = g'_{\Delta\Delta} \equiv g'_{BW}$ , which is the Bäckmann-Weise choice (c.f. Ref. [21] and Refs. therein), one gets  $g'_{BW} = 0.7 \pm 0.1$  from the best description of the unnatural parity isovector states in  ${}^4\text{He}$ ,  ${}^{16}\text{O}$  and  ${}^{40}\text{Ca}$ . However,

the same calculations within the Migdal model [22] assumption  $g'_{N\Delta} = g'_{\Delta\Delta} = 0$  produce  $g'_{NN} = 0.9 \div 1$ . The description of the quenching of the Gamow-Teller matrix elements requires  $g'_{\Delta\Delta} = 0.6 \div 0.7$  (assuming  $g'_{N\Delta} = g'_{\Delta\Delta}$ ) [23]. From the real part of the pion optical potential in  $\pi$ -atoms one gets  $g'_{N\Delta} = 0.2$  and  $g'_{\Delta\Delta} = 0.8$  [22]. The pion induced two-proton emission is the best described with  $g'_{N\Delta} = 0.25 \div 0.35$  [24]. We will adopt the two sets of the Landau-Migdal parameters from Ref. [25] (see Table 1).

As a first step, we calculate the  $NN \rightarrow N\Delta$  cross section in vacuum. The in-medium corrections are introduced in a second step.

### A. Vacuum cross section

The differential  $N_1 N_2 \rightarrow N_3 \Delta_4$  cross section can be written as:

$$d\sigma = (2\pi)^4 \delta^{(4)}(p_1 + p_2 - p_3 - p_4) \overline{|T|^2} \frac{(2m_N)^3 2M_\Delta}{4I} \frac{d^3 p_3}{(2\pi)^3 2\varepsilon_3} \frac{d^3 p_4}{(2\pi)^3 2\varepsilon_4} \mathcal{A}_\Delta(M_\Delta^2) dM_\Delta^2 , \quad (4)$$

where  $\overline{|T|^2}$  is the square of the absolute value of the reaction amplitude  $T$  in the normalization of Ref. [26] averaged over spins of incoming particles 1,2 and summed over spins of outgoing particles 3,4. The flux factor is :  $I \equiv \sqrt{(p_1 p_2)^2 - m_N^4}$ . The spectral function of the  $\Delta$  resonance

$$\mathcal{A}_\Delta(M_\Delta^2) = \frac{1}{\pi} \frac{M_\Delta \Gamma_\Delta(M_\Delta)}{(M_\Delta^2 - m_\Delta^2)^2 + M_\Delta^2 \Gamma_\Delta^2(M_\Delta)} , \quad (5)$$

where  $m_\Delta = 1.232$  GeV is the  $\Delta$  pole mass, satisfies the normalization condition :

$$\int_{(m_N + m_\pi)^2}^{\infty} dM_\Delta^2 \mathcal{A}_\Delta(M_\Delta^2) = 1 . \quad (6)$$

The mass dependent total  $\Delta$  width  $\Gamma_\Delta(M_\Delta)$  is parameterized according to Ref. [27] :

$$\Gamma_\Delta(M_\Delta) = \Gamma_\Delta^0 \left( \frac{q(M_\Delta, m_N, m_\pi)}{q(m_\Delta, m_N, m_\pi)} \right)^3 \frac{m_\Delta \beta_0^2 + q^2(m_\Delta, m_N, m_\pi)}{M_\Delta \beta_0^2 + q^2(M_\Delta, m_N, m_\pi)} , \quad (7)$$

where  $\Gamma_\Delta^0 = 0.118$  GeV is the width at the pole mass,  $\beta_0 = 0.2$  GeV/c is the cut-off parameter. In Eq.(7) and below

$$q(m, m_1, m_2) = \sqrt{\frac{(m^2 + m_1^2 - m_2^2)^2}{4m^2} - m_1^2} \quad (8)$$

is the center-of-mass (c.m.) momentum of outgoing particles with masses  $m_1$  and  $m_2$  from the decay of a particle with mass  $m$ . In the c.m. frame of colliding nucleons one gets after

standard transformations :

$$\frac{d\sigma}{dM_\Delta^2 d\Omega} = \frac{(2m_N)^3 2M_\Delta}{64\pi^2 s} \frac{q(\sqrt{s}, M_\Delta, m_N)}{|T|^2} \frac{q(\sqrt{s}, m_N, m_N)}{q(\sqrt{s}, m_N, m_N)} \mathcal{A}_\Delta(M_\Delta^2) , \quad (9)$$

where  $s = (p_1 + p_2)^2$ .

The amplitude  $T$  is evaluated from the graphs shown in Fig. 1. In order to preserve the symmetry of the cross section with respect to  $\Theta_{c.m.} = 90^\circ$  we have included the contact interaction both in the direct and in the exchange diagrams. The same was done in Refs. [15, 28] whereas in Ref. [24] the contact interaction has been included in the direct term only. For the discussion on this subject we refer the reader to the Appendix of Ref. [28]. Applying Feynman rules with the Lagrangians (1)-(3) one gets the following expressions for the direct (a) and exchange (b) terms of the amplitude :

$$iT_a = [\chi_\Delta^\dagger(4)\Gamma_j^{abs}(k)\chi(2)]iD^{(0)}(k)[\chi^\dagger(3)\Gamma_j^{dec}(k)\chi(1)] - iV_{4,3;2,1}(k) , \quad (10)$$

$$iT_b = -[\chi_\Delta^\dagger(4)\Gamma_j^{abs}(k')\chi(1)]iD^{(0)}(k')[\chi^\dagger(3)\Gamma_j^{dec}(k')\chi(2)] + iV_{4,3;1,2}(k') . \quad (11)$$

Here  $\chi$  and  $\chi_\Delta$  are the spin-isospin wave functions of the nucleon and delta :

$$\chi = \delta_{m_t m} \delta_{\lambda s} , \quad \chi_\Delta = \delta_{M_t M} \delta_{\lambda_\Delta s_\Delta} , \quad (12)$$

where  $m_t = \pm 1/2$  ( $M_t = \pm 3/2, \pm 1/2$ ) and  $\lambda = \pm 1/2$  ( $\lambda_\Delta = \pm 3/2, \pm 1/2$ ) are the quantum numbers of the third isospin and spin component of a nucleon (delta). The quantities  $m$ ,  $s$ ,  $M$  and  $s_\Delta$  are the corresponding indices of the wave functions. The four-momenta of the exchange pion in the direct and exchange channels are  $k = p_1 - p_3$  and  $k' = p_2 - p_3$ , respectively. Below we use the kinematical invariants  $t = k^2$  and  $u = k'^2$ . The operators

$$\Gamma_j^{abs}(k) = -\frac{f_\Delta(t)}{m_\pi} (\mathbf{S} \cdot \mathbf{k}) T_j , \quad (13)$$

$$\Gamma_j^{dec}(k) = \frac{f(t)}{m_\pi} (\boldsymbol{\sigma} \cdot \mathbf{k}) \tau_j \quad (14)$$

represent the  $\pi N \rightarrow \Delta$  absorption and  $N \rightarrow \pi N$  decay vertices in vacuum. The quantity

$$V_{4,3;2,1}(k) = \frac{f_\Delta(t)f(t)}{m_\pi^2} g'_{N\Delta} [\chi_\Delta^\dagger(4)S_\alpha \mathbf{T} \chi(2)][\chi^\dagger(3)\sigma_\alpha \boldsymbol{\tau} \chi(1)] \quad (15)$$

is the contact interaction in vacuum and

$$D^{(0)}(k) = \frac{1}{k^2 - m_\pi^2 + i0} \quad (16)$$

is the free pion propagator. In the  $\pi NN$  and  $\pi N\Delta$  vertices we use the monopole form factor  $F$  :

$$f(t) = fF(t) , \quad f_\Delta(t) = f_\Delta F(t) , \quad F(t) = \frac{\Lambda^2 - m_\pi^2}{\Lambda^2 - t} \quad (17)$$

with  $\Lambda$  being the cut-off parameter (see Table 1). Following Refs. [15, 20] a factor  $F^2$  is included in the contact interaction vertices, since these vertices simulate the exchange by some heavy meson.

The matrix element squared is

$$|T|^2 = |T_a + T_b|^2 = |T_a|^2 + |T_b|^2 + T_a T_b^* + T_a^* T_b . \quad (18)$$

We now consider the case of the  $pp \rightarrow n\Delta^{++}$  reaction. The spin-averaged direct term in (18) is

$$\frac{1}{4} \sum_{\lambda_1, \lambda_2, \lambda_3, \lambda_{\Delta 4}} |T_a|^2 = \frac{4}{3} \left( \frac{f_\Delta(t) f(t)}{m_\pi^2} \right)^2 [\mathbf{k}^4 D^{(0)2}(k) + 2\mathbf{k}^2 D^{(0)}(k) g'_{N\Delta} + 3(g'_{N\Delta})^2] . \quad (19)$$

The spin-averaged exchange term  $\frac{1}{4} \sum_{\lambda_1, \lambda_2, \lambda_3, \lambda_{\Delta 4}} |T_b|^2$  is given by Eq. (19) with replacements  $k \rightarrow k'$  and  $t \rightarrow u$ . The spin-averaged interference term can be written as follows :

$$\begin{aligned} \frac{1}{4} \sum_{\lambda_1, \lambda_2, \lambda_3, \lambda_{\Delta 4}} [T_a T_b^* + T_a^* T_b] &= -\frac{f_\Delta(t) f(t) f_\Delta(u) f(u)}{2m_\pi^4} \left[ \frac{4}{3} ((\mathbf{k} \cdot \mathbf{k}')^2 + \mathbf{k}^2 \mathbf{k}'^2) D^{(0)}(k) D^{(0)}(k') \right. \\ &+ \left. \frac{16}{3} \mathbf{k}^2 D^{(0)}(k) g'_{N\Delta} + \frac{16}{3} \mathbf{k}'^2 D^{(0)}(k') g'_{N\Delta} + 16(g'_{N\Delta})^2 \right] . \end{aligned} \quad (20)$$

In numerical calculations we also took into account the c.m. and relativistic corrections to the amplitudes (10),(11) (c.f. Ref. [28]) : (i) We replaced in (13)  $(\mathbf{S} \cdot \mathbf{k}) \rightarrow (\mathbf{S} \cdot \mathbf{k}_4)$  and  $(\mathbf{S} \cdot \mathbf{k}') \rightarrow (\mathbf{S} \cdot \mathbf{k}'_4)$  in the direct and exchange terms respectively. Here  $\mathbf{k}_4$  ( $\mathbf{k}'_4$ ) is the momentum of the exchanged pion in the rest frame of  $\Delta$  for the direct (exchange) term :

$$\mathbf{k}_4 = \mathbf{k} + \left( \left( \frac{E_4}{M_\Delta} - 1 \right) \frac{\mathbf{k} \cdot \mathbf{p}_4}{\mathbf{p}_4^2} - \frac{k_0}{M_\Delta} \right) \mathbf{p}_4 , \quad (21)$$

$$\mathbf{k}'_4 = \mathbf{k}' + \left( \left( \frac{E_4}{M_\Delta} - 1 \right) \frac{\mathbf{k}' \cdot \mathbf{p}_4}{\mathbf{p}_4^2} - \frac{k'_0}{M_\Delta} \right) \mathbf{p}_4 . \quad (22)$$

(ii) The direct amplitude  $T_a$  is multiplied by the factor  $(-t/\mathbf{k}^2)^{1/2}$  and the exchange amplitude  $T_b$  by the factor  $(-u/\mathbf{k}'^2)^{1/2}$ . This restores approximately the Lorentz invariance after summation of the amplitude squared over spin projections.

After the c.m. and relativistic corrections Eqs.(19),(20) get slightly modified. We do not show here explicit formulas: they will be given below for the more general in-medium case (see Eqs.(A7),(A8) in Appendix A).

In the upper panel of Fig. 2 we present the total cross section  $\sigma_{pp \rightarrow n\Delta^{++}}$  as a function of the c.m. energy. Dashed and solid lines correspond to the case of Set 1 and Set 2, respectively; the dotted line represents the relativistic calculation using the model of Ref. [19]. The relativistic and our corrected nonrelativistic calculations are in a good agreement at  $\sqrt{s} < 3$  GeV. At higher c.m. energies our calculations produce somewhat larger cross section than the relativistic result of Ref. [19]. In the lower panel of Fig. 2 we show the total cross section of the process  $\sigma_{pp \rightarrow p\pi^+}$  vs the c.m. energy in comparison to the data from Ref. [29]. In this case the dominating channel is still  $\sigma_{pp \rightarrow n\Delta^{++}}$ ,  $\Delta^{++} \rightarrow p\pi^+$ , however, also other channels contribute:  $\sigma_{pp \rightarrow p\Delta^+}$ ,  $\Delta^+ \rightarrow n\pi^+$ , which has a cross section of 1/9 of the one for the channel through the  $\Delta^{++}$  production; channels with higher resonance excitation [7], whose contributions are shown by long-dashed and dash-dotted lines for the isospin 1/2 and 3/2 resonances, respectively; the nonresonant (background) *s*-wave channel  $pp \rightarrow np\pi^+$  [7] shown by short-dashed line. The sum of all contributions in the case of our  $pp \rightarrow n\Delta^{++}$  cross section calculated with the Set 2 and in the case of the cross section from Ref. [19] is shown by the solid and dotted lines, respectively. The experimental data are well described in both cases. For  $\sqrt{s} < 3$  GeV the Set 2 is a little closer to the data, while for higher c.m. energies the relativistic calculation of Ref. [19] works somewhat better. For the practical applications the difference at high c.m. energies is not important, since anyway the FRITIOF model is applied for the baryon-baryon collisions at  $\sqrt{s} > 2.6$  GeV in the BUU program [27] which we use in the description of pion production from heavy-ion collisions.

Since our major goal is to describe the pion production from heavy-ion collisions at the beam energies  $\sim 1$  A GeV, we have also checked the differential cross sections  $pp \rightarrow np\pi^+$  at  $p_{lab} = 1.66$  GeV/c ( $E_{lab} = 0.97$  GeV). Fig. 3 shows the c.m. polar angle distribution of neutrons. Our calculation is again in a very close agreement with the relativistic treatment of Ref. [19] and describes the data [30] well. We neglected the contribution of the channel  $pp \rightarrow p\Delta^+$ ,  $\Delta^+ \rightarrow \pi^+n$  in comparison to the data: taking into account this channel would roughly multiply our results by a factor of 10/9, which would yield an even better agreement with the data. The invariant mass distribution of  $(\pi^+, p)$  pairs is shown in Fig. 4. We see that both models agree quite well, but the experimental distribution from [30] is somewhat broader. Notice, that the channel  $pp \rightarrow p\Delta^+$ ,  $\Delta^+ \rightarrow \pi^+n$  missed in our calculations would create some broadening of the spectrum, since now the pair  $(\pi^+, p)$  is not emitted from the same resonance. However, the study of this effect is beyond the scope of our work.

## B. In-medium corrections

### 1. Effective masses and in-medium $\Delta$ width

We assume that nucleons and  $\Delta$ 's are coupled to the scalar mean field  $\sigma$  by the same universal coupling constant  $g_\sigma$  [31]. This produces the Dirac effective masses

$$m_N^* = m_N + g_\sigma \sigma, \quad m_\Delta^* = m_\Delta + g_\sigma \sigma, \quad (23)$$

which are smaller than the bare ones by  $300 \div 400$  MeV at the normal nuclear density, as one can see from Fig. 5. We have adopted the two parameter sets of the relativistic mean field model (RMF) [32]: NL1 and NL2, and the Relativistic Hartree Approximation (RHA) [33]. RHA takes into account vacuum fluctuations which are missed in RMF. We observe from Fig. 5, that the RMF set NL1 produces the steepest decrease of the nucleon effective mass with the baryon density, while RHA gives the slowest one.

Assuming, further, that the coupling constants to the vector mean field  $\omega$  are also the same for nucleons and  $\Delta$ 's [31], we get the kinetic four-momenta

$$p_N^* = p_N - g_\omega \omega, \quad p_\Delta^* = p_\Delta - g_\omega \omega. \quad (24)$$

The effective masses and the kinetic four-momenta substitute the vacuum masses and four-momenta in the calculations. Thus, in Eq. (4) one should replace :

$$p_i \rightarrow p_i^*, \quad i = 1, 2, 3, 4, \quad (25)$$

$$m_N \rightarrow m_N^*, \quad (26)$$

$$M_\Delta \rightarrow M_\Delta^*, \quad (27)$$

$$I \rightarrow I^* = \sqrt{(p_1^* p_2^*)^2 - m_N^{*4}}, \quad (28)$$

$$\mathcal{A}_\Delta(M_\Delta^2) \rightarrow \mathcal{A}_\Delta^*(M_\Delta^{*2}) = \frac{1}{\pi} \frac{M_\Delta^* \Gamma_\Delta^*(M_\Delta^*)}{(M_\Delta^{*2} - m_\Delta^{*2})^2 + M_\Delta^{*2} \Gamma_\Delta^{*2}(M_\Delta^*)}. \quad (29)$$

The total in-medium  $\Delta$  width is approximated as follows :

$$\Gamma_\Delta^*(M_\Delta^*) = \Gamma_{sp} \frac{\rho}{\rho_0} + \Gamma_\Delta^0 \left( \frac{q(M_\Delta^*, m_N^*, m_\pi)}{q(m_\Delta, m_N, m_\pi)} \right)^3 \frac{m_\Delta^* \beta_0^2 + q^2(m_\Delta^*, m_N^*, m_\pi)}{M_\Delta^* \beta_0^2 + q^2(M_\Delta^*, m_N^*, m_\pi)}, \quad (30)$$

where  $\rho_0 = 0.16$  fm $^{-3}$  is the nuclear saturation density and  $\Gamma_{sp}$  is a constant. The first term in Eq.(30) is the  $\Delta$ -spreading width [34, 35], which describes the in-medium broadening of the  $\Delta$  resonance due to the absorption and rescattering processes  $\Delta N \rightarrow NN$ ,  $\Delta N \rightarrow \Delta N$

and  $\Delta NN \rightarrow NNN$ . In Ref. [35] the many-body calculations of the  $\Delta$  self-energy in nuclear matter have been performed which are in a good agreement with the empirical  $\Delta$ -spreading potential of Ref. [34]

$$W_{sp} = (23 \pm 5) - i(43 \pm 5) \frac{\rho}{\rho_0} \text{ (MeV)} . \quad (31)$$

Thus, the value of the constant  $\Gamma_{sp}$  consistent with Refs. [34, 35] is  $\Gamma_{sp} = -2\text{Im}W_{sp}(\rho = \rho_0) = 80$  MeV. In Ref. [36] another value  $\Gamma_{sp} = 20$  MeV has been used in the calculation of the pion self-energy within the  $\Delta$ -hole model. In Ref. [37] the  $\Delta$ -spreading width has been calculated in the relativistic meson-nucleon model including effective masses given by the Walecka model. Only the  $\Delta N \rightarrow NN$  contribution has been taken into account. Vertex corrections were neglected in Ref. [37], which resulted in rather big values of the  $\Delta$ -spreading width in the calculation without effective mass ( $\Gamma_{sp} = 160$  MeV). Including effective mass corrections, the  $\Delta$ -spreading width of Ref. [37], first, increases with density at  $\rho < \rho_0$  in agreement with  $\Gamma_{sp} = 80$  MeV, but then drops abruptly at higher densities due to the mean field effects. We have checked that the variation of the parameter  $\Gamma_{sp}$  within the range  $0 \div 80$  MeV leads to the changes in the in-medium cross section  $NN \rightarrow N\Delta$  which are comparable with the ambiguity due to the choice of the effective mass parameterization (NL1 or NL2). On the other hand, we need to keep  $\Gamma_{sp} \neq 0$  in order to have numerically stable results in the calculations of the  $\Delta$ -hole Lindhard function (44). In the numerical results presented below we use  $\Gamma_{sp} = 80$  MeV.

The second term in Eq.(30) is the  $\Delta \rightarrow N\pi$  width taking into account the effective masses of the nucleon and  $\Delta$ . In this term we have omitted the Pauli blocking of the decay nucleon. This is justified because in the real heavy-ion collision at the beam energy of 1 A GeV the nuclear matter at finite temperature of about 70 MeV is created, which reduces the Pauli blocking effect strongly with respect to the zero temperature nuclear matter.

In the c.m. frame of colliding nucleons (i.e. in the frame where  $\mathbf{p}_1^* + \mathbf{p}_2^* = 0$ ) the differential cross section in nuclear medium reads as follows (c.f. (9)) :

$$\frac{d\sigma^{med}}{dM_\Delta^{*2} d\Omega} = \frac{(2m_N^*)^3 2M_\Delta^*}{64\pi^2 s^*} \frac{q(\sqrt{s^*}, M_\Delta^*, m_N^*)}{|T^{med}|^2} \frac{q(\sqrt{s^*}, m_N^*, m_N^*)}{\mathcal{A}_\Delta(M_\Delta^{*2})} , \quad (32)$$

where  $s^* = (p_1^* + p_2^*)^2$ . Below we will assume that the c.m. frame of colliding particles coincides with the nuclear matter rest frame, where spatial components of the vector field disappear, thus  $\mathbf{p}^* = \mathbf{p}$ .

## 2. Pion self-energy

The in-medium matrix element  $T^{med}$  in Eq. (32) is given by the graphs shown in Fig. 1, where now the in-medium pion propagator

$$D(k) = \frac{1}{k^2 - m_\pi^2 - \Pi(k)} \quad (33)$$

must be put on the place of the vacuum propagator  $D^{(0)}(k)$  and the in-medium vertex corrections due to the contact interactions must be also taken into account. The pion self-energy  $\Pi_{ab}(k)$  is, in general, a matrix with two isospin indices  $a, b = 1, 2, 3$ . However, in this Section we consider isospin-symmetric nuclear matter, where  $\Pi_{ab}(k) = \delta_{ab}\Pi(k)$ . The delta function of the isospin indices will be always dropped below for brevity. The assumption of isospin-symmetric nuclear matter results, in particular, in the validity of the vacuum relations between various isospin channels (c.f Eqs.(56),(57) below) for the in-medium cross sections. To avoid misunderstanding, we stress, however, that in the BUU calculations of Sect. III we take into account the isospin assymmetry of colliding nuclei explicitly.

The function  $-i\Pi(k) = -i\Pi_\Delta(k) - i\Pi_N(k)$  is shown in Fig. 6a. It includes the  $\Delta$ -hole and nucleon-hole iterated contributions: we denoted them as  $-i\Pi_\Delta(k)$  and  $-i\Pi_N(k)$  respectively. These contributions satisfy the recurrence relations shown in Fig. 6b,c which read as :

$$\hat{A}(k) \begin{pmatrix} \Pi_N(k) \\ \Pi_\Delta(k) \end{pmatrix} = -\mathbf{k}^2 \begin{pmatrix} \chi_N(k) \\ \chi_\Delta(k) \end{pmatrix}, \quad (34)$$

where the  $2 \times 2$  matrix  $\hat{A}(k)$  is

$$\hat{A}(k) \equiv \begin{pmatrix} 1 + g'_{NN}\chi_N(k) & g'_{N\Delta}\chi_N(k) \\ g'_{N\Delta}\chi_\Delta(k) & 1 + g'_{\Delta\Delta}\chi_\Delta(k) \end{pmatrix}. \quad (35)$$

The susceptibilities  $\chi_N(k)$  and  $\chi_\Delta(k)$  are :

$$\chi_N(k) = \frac{4f^2(k^2)}{m_\pi^2}\phi(k), \quad (36)$$

$$\chi_\Delta(k) = \frac{16f_\Delta^2(k^2)}{9m_\pi^2}(\phi_\Delta(k) + \phi_\Delta(-k)) \quad (37)$$

with  $\phi(k)$  and  $\phi_\Delta(\pm k)$  being, respectively, the nucleon-hole and  $\Delta$ -hole Lindhard functions :

$$\phi(k) = i \int \frac{d^4p}{(2\pi)^4} G(p)G(p+k), \quad (38)$$

$$\phi_\Delta(\pm k) = i \int \frac{d^4p}{(2\pi)^4} G(p)G_\Delta(p \pm k). \quad (39)$$

Here  $G(p)$  and  $G_\Delta(p_\Delta)$  are the nucleon and  $\Delta$  propagators :

$$G(p) = \frac{1}{p^0 - \varepsilon^*(\mathbf{p}) + i0} + 2\pi i n(\mathbf{p})\delta(p^0 - \varepsilon^*(\mathbf{p})) , \quad (40)$$

$$G_\Delta(p_\Delta) = \frac{1}{p_\Delta^0 - \varepsilon_\Delta^*(\mathbf{p}_\Delta) + i\Gamma_\Delta^*(\sqrt{p_\Delta^2})/2} , \quad (41)$$

where

$$\varepsilon^*(\mathbf{p}) = \sqrt{\mathbf{p}^2 + (m_N^*)^2} , \quad \varepsilon_\Delta^*(\mathbf{p}_\Delta) = \sqrt{\mathbf{p}_\Delta^2 + (m_\Delta^*)^2} \quad (42)$$

are the on-shell nucleon and  $\Delta$  energies,  $n(\mathbf{p})$  is the nucleon occupation number. The nucleon propagator (40) consists of the vacuum part and the in-medium part ( $\propto n(\mathbf{p})$ ). The  $\Delta$  propagator (41) includes the vacuum part only, since we have neglected the presence of  $\Delta$  excitations in nuclear matter. Both propagators take into account the effective mass corrections.

After the contour integration over  $p^0$  (c.f. [38]) the nucleon-hole Lindhard function (38) takes the following form :

$$\phi(k) = - \int \frac{d^3p}{(2\pi)^3} \left( \frac{n(\mathbf{p} + \mathbf{k})(1 - n(\mathbf{p}))}{\varepsilon^*(\mathbf{p} + \mathbf{k}) - k^0 - \varepsilon^*(\mathbf{p}) + i0} + \frac{n(\mathbf{p})(1 - n(\mathbf{p} + \mathbf{k}))}{\varepsilon^*(\mathbf{p}) + k^0 - \varepsilon^*(\mathbf{p} + \mathbf{k}) + i0} \right) . \quad (43)$$

We have used the analytic formulas given in Ref. [38] for the calculation of the integral (43) in the case of Fermi distribution at zero temperature  $n(\mathbf{p}) = \Theta(p_F - |\mathbf{p}|)$ .

The  $\Delta$ -hole Lindhard function (39), after integration over  $p^0$ , can be expressed as

$$\phi_\Delta(\pm k) = - \int \frac{d^3p}{(2\pi)^3} \frac{n(\mathbf{p})}{\varepsilon^*(\mathbf{p}) \pm k^0 - \varepsilon_\Delta^*(\mathbf{p} \pm \mathbf{k}) + i\Gamma_\Delta^*(\sqrt{(p^*)^2 + k^2})/2} , \quad (44)$$

where  $p^* \equiv (\varepsilon^*(\mathbf{p}), \mathbf{p})$ . In the calculation of the integral (44) we have used the expression from the Appendix of Ref. [39] (see also the Appendix in Ref. [40]) assuming that the invariant mass of the nucleon and pion in the argument of  $\Gamma^*$  can be approximated by

$$(p^*)^2 \simeq (m_N^*)^2 + k^2 \pm 2k^0 \sqrt{(m_N^*)^2 + \frac{3}{5}p_F^2} . \quad (45)$$

Solving the system (34) we get for the pion self-energy the following expression :

$$\begin{aligned} \Pi(k) &= \Pi_\Delta(k) + \Pi_N(k) = -\mathbf{k}^2 \det^{-1}(\hat{A}(k)) \\ &\times [(1 + g'_{\Delta\Delta}\chi_\Delta(k))\chi_N(k) + (1 + g'_{NN}\chi_N(k))\chi_\Delta(k) - 2g'_{N\Delta}\chi_N(k)\chi_\Delta(k)] , \end{aligned} \quad (46)$$

where

$$\det(\hat{A}(k)) = (1 + g'_{NN}\chi_N(k))(1 + g'_{\Delta\Delta}\chi_\Delta(k)) - (g'_{N\Delta})^2\chi_N(k)\chi_\Delta(k) . \quad (47)$$

Expression (46) coincides with the result from Ref. [41].

### 3. Vertex corrections

The renormalized  $\pi N \rightarrow \Delta$  absorption vertex operator  $\tilde{\Gamma}_j^{abs}(k)$  is shown in Fig. 7a. The first graph in Fig. 7a is the  $\pi N \rightarrow \Delta$  absorption vertex operator in vacuum  $\Gamma_j^{abs}(k)$  (see Eq.(13)). The second and third graphs in Fig. 7a correspond to the iterated nucleon-hole and  $\Delta$ -hole corrections which we will denote as  $\tilde{\Gamma}_{j,N}^{abs}(k)$  and  $\tilde{\Gamma}_{j,\Delta}^{abs}(k)$  respectively. The correction terms satisfy the recurrence relations shown in Fig. 7b,c which can be written as :

$$\hat{A}(k) \begin{pmatrix} \tilde{\Gamma}_{j,N}^{abs}(k) \\ \tilde{\Gamma}_{j,\Delta}^{abs}(k) \end{pmatrix} = -\Gamma_j^{abs}(k) \begin{pmatrix} g'_{N\Delta}\chi_N(k) \\ g'_{\Delta\Delta}\chi_\Delta(k) \end{pmatrix}. \quad (48)$$

After solution of the system (48) we obtain the expression for the operator  $\tilde{\Gamma}_j^{abs}(k)$  :

$$\begin{aligned} \tilde{\Gamma}_j^{abs}(k) &= \Gamma_j^{abs}(k) + \tilde{\Gamma}_{j,N}^{abs}(k) + \tilde{\Gamma}_{j,\Delta}^{abs}(k) \\ &= \det^{-1}(\hat{A}(k))[1 + (g'_{NN} - g'_{N\Delta})\chi_N(k)]\Gamma_j^{abs}(k). \end{aligned} \quad (49)$$

In an analogous way, the renormalized  $N \rightarrow \pi N$  decay vertex operator  $\tilde{\Gamma}_j^{dec}(k)$  can be represented as a sum of the vacuum operator  $\Gamma_j^{dec}(k)$ , the iterated nucleon-hole  $\tilde{\Gamma}_{j,N}^{dec}(k)$  and  $\Delta$ -hole  $\tilde{\Gamma}_{j,\Delta}^{dec}(k)$  contributions (see Fig. 8a). The recurrence relations for  $\tilde{\Gamma}_{j,N}^{dec}(k)$  and  $\tilde{\Gamma}_{j,\Delta}^{dec}(k)$  are shown in Fig. 8b,c. Algebraically, they look as :

$$\hat{A}(k) \begin{pmatrix} \tilde{\Gamma}_{j,N}^{dec}(k) \\ \tilde{\Gamma}_{j,\Delta}^{dec}(k) \end{pmatrix} = -\Gamma_j^{dec}(k) \begin{pmatrix} g'_{NN}\chi_N(k) \\ g'_{N\Delta}\chi_\Delta(k) \end{pmatrix}. \quad (50)$$

Resolving (50) one gets the renormalized vertex operator  $\tilde{\Gamma}_j^{dec}(k)$  :

$$\begin{aligned} \tilde{\Gamma}_j^{dec}(k) &= \Gamma_j^{dec}(k) + \tilde{\Gamma}_{j,N}^{dec}(k) + \tilde{\Gamma}_{j,\Delta}^{dec}(k) \\ &= \det^{-1}(\hat{A}(k))[1 + (g'_{\Delta\Delta} - g'_{N\Delta})\chi_\Delta(k)]\Gamma_j^{dec}(k). \end{aligned} \quad (51)$$

Finally, Fig. 9a shows the renormalized contact interaction  $-i\tilde{V}(k)$  (we drop here the indices of external particles for brevity) given by the sum of the bare contact interaction  $-iV(k)$ , nucleon-hole  $-i\tilde{V}_N(k)$  and  $\Delta$ -hole  $-i\tilde{V}_\Delta(k)$  iterated contributions. The recurrence relations for  $-i\tilde{V}_N(k)$  and  $-i\tilde{V}_\Delta(k)$ , shown graphically in Fig. 9b,c, are :

$$\begin{pmatrix} 1 + g'_{NN}\chi_N(k) & g'_{NN}\chi_N(k) \\ \frac{(g'_{N\Delta})^2}{g'_{NN}}\chi_\Delta(k) & 1 + g'_{\Delta\Delta}\chi_\Delta(k) \end{pmatrix} \begin{pmatrix} \tilde{V}_N(k) \\ \tilde{V}_\Delta(k) \end{pmatrix} = -V(k) \begin{pmatrix} g'_{NN}\chi_N(k) \\ g'_{\Delta\Delta}\chi_\Delta(k) \end{pmatrix}. \quad (52)$$

Resolving the system (52) we get a simple formula for  $\tilde{V}(k)$  :

$$\tilde{V}(k) = V(k) + \tilde{V}_N(k) + \tilde{V}_\Delta(k) = \det^{-1}(\hat{A}(k))V(k) . \quad (53)$$

The in-medium matrix element  $T^{med}$  is given by the sum of the direct Eq.(10) and exchange Eq.(11) contributions where  $\Gamma$  and  $V$  are replaced by the renormalized quantities. The explicit formulas for calculation of  $|\overline{T^{med}}|^2$  are given in Appendix A.

#### 4. Cross sections

Fig. 10 shows the total in-medium  $pp \rightarrow n\Delta^{++}$  cross section vs the c.m. kinetic energy above the pion production threshold

$$Q^* = \sqrt{s^*} - 2m_N^* - m_\pi \quad (54)$$

for different densities. We compare the cross sections at fixed  $Q^*$  rather than at fixed c.m. momentum, because  $Q^*$  is the direct measure of the collision inelasticity: e.g.,  $\sigma_{pp \rightarrow n\Delta^{++}}^{med}(Q^* = 0) = 0$  for all baryon densities, while the threshold value of the c.m. momentum is density dependent. The solid lines in the panels a,b and c of Fig. 10 show the results of the full calculation (i.e. including effective masses, the pion collectivity and vertex renormalization) for the combinations NL1-Set1, NL1-Set2 and NL2-Set2, respectively. We see that the cross section quickly drops with baryon density. The strongest effect is obtained for the combination NL1-Set2: in this case  $\sigma_{pp \rightarrow n\Delta^{++}}^{med}$  drops by two orders of magnitude when the density increases from 0 up to  $3\rho_0$ . The combination NL1-Set1 produces a somewhat weaker decrease of  $\sigma_{pp \rightarrow n\Delta^{++}}^{med}$  with density than the combination NL1-Set2. However, an effect of the choice of the OPEM parameters on the result is much smaller than the effect of the choice of the effective nucleon and  $\Delta$  masses. The set NL2 gives less in-medium reduction than the set NL1 as one expects from Fig. 5.

The main reason for the in-medium reduction of the cross section is the factor of  $(2m_N^*)^3 2M_\Delta^*/s^*$  in front of the matrix element squared in Eq. (32) for the differential cross section. To demonstrate this, we have repeated the calculation using the NL2-Set2 combination replacing this factor by its vacuum value, i.e.  $(2m_N^*)^3 2M_\Delta^*/s^* \rightarrow (2m_N)^3 2M_\Delta/s$  (see dashed lines in the panel c of Fig. 10). One observes that the cross section calculated with the vacuum factor practically does not depend on the density. Further replacements of

the c.m. momenta of the incoming and outgoing particles by their vacuum values and also of the effective by vacuum masses in the spectral function in Eq. (32) have no any visible effect.

In order to better understand the reason for the lack of the density dependence in the calculation with the vacuum phase space factor we have also calculated the cross section using the Set2 of the OPEM parameters with vacuum masses both in the matrix element and phase space factors (panels e and f of Fig. 10). Panels e and f of Fig. 10 show the results with and without pion collectivity and vertex renormalization effects, respectively. Namely, in the calculation presented in panel f we have put all the Lindhard functions equal to zero. However, the  $\Delta$ -spreading width is still present in the results shown in panels e and f. (i) As one can see from panel e, the cross section drops with density even without any inclusion of the effective masses. By comparing the solid lines in panel e with the dashed lines in panel c we conclude that the inclusion of the effective masses in the matrix element increases the cross section. (ii) From panel f we observe that the  $\Delta$ -spreading width in the spectral function reduces the cross section slightly. As discussed above, this effect is comparable with the ambiguity given by the choice of the effective mass parameterization. (iii) By comparing the curves in panels e and f one sees that the pion collectivity and vertex renormalization reduce the cross section rather noticeably. Therefore, the density independence observed for the calculation with the vacuum phase space factor only (dashed lines in panel c) is, basically, due to a counterbalance of the effects (i) and (iii).

Panel d of Fig. 10 shows the NL2-Set2 calculation with the Lindhard functions putted to zero in the matrix element (solid lines) and also the calculation using the matrix element of Ref. [19] with the in-medium nucleon and  $\Delta$  masses from the NL2 set (dashed lines). As expected, both calculations are in a very close agreement since the nucleon-hole and  $\Delta$ -hole Lindhard functions are absent in both cases.

A comment is in order here on the relation to the results of Ref. [15] where it was shown neglecting effective mass corrections that the in-medium cross section  $\sigma_{pp \rightarrow n\Delta^{++}}^{med}$  grows with baryon density. We have repeated the calculations of [15] with the parameter set B ( $\Lambda = 0.565$  GeV,  $g'_{N\Delta} = 1/3$ ) for the proton beam energy  $E_{lab} = 0.8$  GeV. Following Ref. [15] we have kept only the  $\Delta$ -hole Lindhard function in the quasistatic approximation with

zero width of the  $\Delta$  resonance

$$\chi_{\Delta}(k) \simeq -\frac{8f_{\Delta}^2(k^2)}{9m_{\pi}^2}\rho \frac{\omega_{\Delta}}{(k^0)^2 - \omega_{\Delta}^2}, \quad (55)$$

where  $\omega_{\Delta} = m_{\Delta} - m_N + \mathbf{k}^2/(2m_{\Delta})$ . In the  $\Delta$  spectral function the  $\Delta$  width has been also put to zero [15]. Within these approximations we have reproduced the result of Ref. [15] on the in-medium enhancement of  $\sigma_{pp \rightarrow n\Delta^{++}}^{med}$  (see crosses in Fig. 11). The inclusion of the in-medium  $\Delta$  width reduces the in-medium enhancement (see filled boxes in Fig. 11), which has been also demonstrated earlier in Ref. [16]. We have found that taking into account the nucleon-hole Lindhard function makes  $\sigma_{pp \rightarrow n\Delta^{++}}^{med}$  a decreasing function of the density at  $\rho > \rho_0$  in the calculations with vacuum masses (filled circles in Fig. 11). In the calculations with effective masses the nucleon-hole Lindhard function has a very small effect. For the choice of the Landau-Migdal parameters and of the cut-off factor from Set2 the cross section decreases faster with density (triangles in Fig. 11). Introducing the effective masses amplifies the in-medium reduction effect strongly (see rombuses in Fig. 11).

Summarizing all these findings, we can state that by just changing the factor in front of the matrix element in (9) to its in-medium value takes care of most of the in-medium corrections on the  $\Delta$ -production cross section. This finding offers a way that can easily be implemented into any numerical realization.

In Fig. 12 we show the in-medium differential cross section of the outgoing neutron at various densities for  $Q^* = 0.295$  GeV which corresponds to  $p_{lab} = 1.66$  GeV/c at  $\rho = 0$ . For the calculation without effective mass (lower right panel) the shape of the angular distribution does not depend, practically, on the density for  $60^\circ < \Theta_{cm} < 120^\circ$ : only changes for forward/backward angles are visible. However, in the calculations with effective masses (all other panels) the cross section becomes more isotropic with increasing density in qualitative agreement with the Dirac-Brueckner calculations of the elastic NN cross section in nuclear matter [42, 43].

### III. BUU CALCULATIONS

The in-medium modified  $pp \rightarrow n\Delta^{++}$  cross section has been implemented in the BUU program of the version described in Ref. [27]. More details can be found in Ref. [44]. The cross sections for another isospin channels are related to the  $pp \rightarrow n\Delta^{++}$  cross section by

the Clebsch-Gordan coefficients which gives:

$$\sigma_{pp \rightarrow p\Delta^+}^{med} = \sigma_{pn \rightarrow p\Delta^0}^{med} = \sigma_{pn \rightarrow n\Delta^+}^{med} = \sigma_{nn \rightarrow n\Delta^0}^{med} = \frac{1}{3} \sigma_{pp \rightarrow n\Delta^{++}}^{med} , \quad (56)$$

$$\sigma_{nn \rightarrow p\Delta^-}^{med} = \sigma_{pp \rightarrow n\Delta^{++}}^{med} . \quad (57)$$

Besides the  $\Delta$ -excitation, there are another channels of the pion production in a NN collision. At collision energies above the pion production threshold  $\sqrt{s} > 2m_N + m_\pi$  not only the  $\Delta(1232)$ , but any other resonance  $R$  can be excited :

$$NN \rightarrow NR , \quad (58)$$

where  $R$  stands for  $N^*(1440)$ ,  $N^*(1535)$ ,  $N^*(1650)$  ... (see Ref. [27] for the full list of resonances implemented in the BUU code). At  $\sqrt{s} > 2(m_N + m_\pi)$  the double  $\Delta$  production channel opens :

$$NN \rightarrow \Delta\Delta . \quad (59)$$

In addition, at collision energies slightly above the pion production threshold the  $s$ -wave direct pion production mechanism is important :

$$NN \rightarrow NN\pi . \quad (60)$$

In analogy with the density modification of the  $\Delta$  resonance cross section, we have also modified the processes (58),(59) and (60) keeping, however, the constant density independent matrix elements as determined in Ref. [7].

For the in-medium cross section for the process (58) we apply Eq. (32), where any higher resonance replaces the  $\Delta$  resonance and  $|\overline{T^{med}}|^2$  is now a constant depending on the isospin channel. The effective mass of a higher resonance  $R$  is supposed to be

$$M_R^* = M_R + g_\sigma \sigma , \quad (61)$$

i.e. we assume the same mass shift for all baryon resonances. The spectral function of a higher resonance  $R$  is given by Eq. (29) with replacement “ $\Delta$ ”  $\rightarrow$  “ $R$ ”, where the medium-modified total width is a sum of partial widths :

$$\Gamma_R^*(M_R^*) = \sum_i \Gamma_{R,i}^*(M_R^*) , \quad (62)$$

$$\Gamma_{R,i}^*(M_R^*) = \Gamma_{R,i}^0 \frac{\rho_i^*(M_R^*)}{\rho_i^*(m_R^*)} , \quad (63)$$

where  $m_R^* = m_R + g_\sigma \sigma$ .  $m_R$  is the pole mass of a resonance  $R$  and

$$\begin{aligned} \rho_i^*(M_R^*) &= \int d(M_B^*)^2 d(M_m)^2 \mathcal{A}_B^*((M_B^*)^2) \\ &\times \mathcal{A}_m((M_m)^2) \frac{q(M_R^*, M_B^*, M_m)}{M_R^*} B_{l_i}^2(q(M_R^*, M_B^*, M_m)/\beta_0) . \end{aligned} \quad (64)$$

Here, the lower indices “ $B$ ” and “ $m$ ” mean the outgoing baryon and meson for the  $i$ -th decay channel:  $(B, m) = (N, \pi), (N, \eta), (N, \omega), (\Lambda, K), (\Delta(1232), \pi), (N, \rho), (N, \sigma), (N(1440), \pi), (\Delta(1232), \rho)$ .  $\mathcal{A}_B^*((M_B^*)^2)$  and  $\mathcal{A}_m((M_m)^2)$  are the spectral functions of the outgoing particles,  $B_{l_i}^2$  is a Blatt-Weisskopf barrier penetration factor corresponding to the relative angular momentum  $l_i$  of the outgoing baryon and meson. Eqs. (62),(63),(64) are the in-medium modification of the vacuum widths from Ref. [27]. We have to remark only, that also for the outgoing  $\Lambda$  we take in Eq. (64) an in-medium spectral function  $\mathcal{A}_\Lambda^*((M_\Lambda^*)^2) \equiv \delta((M_\Lambda^*)^2 - (m_\Lambda + g_\sigma \sigma)^2)$ . This is necessary in order to keep the decay channel  $R \rightarrow \Lambda K$  open in nuclear matter, since the resonance  $R$  has now reduced mass. However, we did not modify any cross sections involving strange particles which is out of scope of our work.

For the in-medium cross section of the process  $NN \rightarrow \Delta\Delta$  we apply the following formula :

$$\begin{aligned} \frac{d\sigma_{N_1 N_2 \rightarrow \Delta_3 \Delta_4}^{med}}{d(M_3^*)^2 d(M_4^*)^2} &= \frac{(2m_N^*)^2 (2m_\Delta^*)^2}{16\pi s^*} \overline{|T_{N_1 N_2 \rightarrow \Delta_3 \Delta_4}|^2} S_{34} \\ &\times \frac{q(\sqrt{s^*}, M_3^*, M_4^*)}{q(\sqrt{s^*}, m_N^*, m_N^*)} \mathcal{A}_\Delta^*((M_3^*)^2) \mathcal{A}_\Delta^*((M_4^*)^2) , \end{aligned} \quad (65)$$

where the matrix element  $\overline{|T_{N_1 N_2 \rightarrow \Delta_3 \Delta_4}|^2}$  depends on the isospins of incoming and outgoing particles only.  $S_{ij} = 1$  ( $1/2$ ) if the  $i$ -th and  $j$ -th particles are in the different (same) isospin states. In the vacuum the cross section (65) is the same as in Ref. [44].

Finally, we have also introduced effective mass modifications for the process of the direct  $s$ -wave pion production  $NN \rightarrow NN\pi$  which can be written in the form of the Dalitz plot [45] :

$$\begin{aligned} d\sigma_{N_1 N_2 \rightarrow N_3 N_4 \pi}^{med} &= \frac{(2m_N^*)^4}{(2\pi)^3 64 q(\sqrt{s^*}, m_N^*, m_N^*) (s^*)^{3/2}} \\ &\times \overline{|T_{N_1 N_2 \rightarrow N_3 N_4 \pi}|^2} (\sqrt{s}) S_{34} d(m_{34}^*)^2 d(m_{4\pi}^*)^2 , \end{aligned} \quad (66)$$

where  $(m_{34}^*)^2 = (p_3^* - p_4^*)^2$  and  $(m_{4\pi}^*)^2 = (p_4^* - k)^2$  are the invariant masses squared of the pairs of outgoing particles  $N_3, N_4$  and  $N_4, \pi$  respectively.  $\overline{|T_{N_1 N_2 \rightarrow N_3 N_4 \pi}|^2} (\sqrt{s})$  is the vacuum

matrix element squared which depends on the vacuum c.m. energy  $\sqrt{s}$  (see Eq.(68) below) and on the isospins of the involved particles. From Eq. (66) one gets the following relation between the in-medium and vacuum cross sections :

$$\begin{aligned}\sigma_{N_1 N_2 \rightarrow N_3 N_4 \pi}^{med}(\sqrt{s^*}) &= \frac{q(\sqrt{s}, m_N, m_N) s^{3/2}}{q(\sqrt{s^*}, m_N^*, m_N^*)(s^*)^{3/2}} \left(\frac{m_N^*}{m_N}\right)^4 \\ &\times \frac{\int d(m_{34}^*)^2 d(m_{4\pi}^*)^2}{\int d(m_{34})^2 d(m_{4\pi})^2} \sigma_{N_1 N_2 \rightarrow N_3 N_4 \pi}^{vac}(\sqrt{s}) ,\end{aligned}\quad (67)$$

where  $\sigma_{N_1 N_2 \rightarrow N_3 N_4 \pi}^{vac}(\sqrt{s})$  is the vacuum cross section parameterized in Ref. [7].

In order to maintain detailed balance, one must modify also the inverse processes  $N\Delta \rightarrow NN$ ,  $NR \rightarrow NN$ ,  $\Delta\Delta \rightarrow NN$ ,  $\pi NN \rightarrow NN$  – which are obviously essential for pion reabsorption – simultaneously with the direct reactions. We collect the formulas for the in-medium cross sections of the inverse processes in Appendix B.

Since the mean field included in the BUU model is a Skyrme-like which is different from the RMF model, a recipe must be found how to match the BUU kinematics of a nucleon-nucleon collision with the kinematics employing Dirac effective masses. One way is to take the incoming particle momenta from BUU and construct  $s^*$  by replacing the bare masses by the effective ones. However, as we discussed in Sect. II, if the c.m. momentum is fixed, a NN collision which is subthreshold for pion production in the vacuum may get above threshold in the nuclear medium. This would create practical difficulties in ensuring energy conservation for the outgoing particles. Therefore, we have used the c.m. kinetic energy above the pion production threshold from BUU as an input to the calculation of the in-medium cross sections. Namely, for each NN collision we find  $Q = \sqrt{s} - 2m_N - m_\pi$ , where  $\sqrt{s}$  is calculated with the incoming nucleon momenta from BUU using the vacuum dispersion relation for nucleon energies. The in-medium c.m. energy  $\sqrt{s^*}$  is determined by requiring that  $Q^* = Q$ , i.e.

$$\sqrt{s^*} = \sqrt{s} - 2(m_N - m_N^*) . \quad (68)$$

Correspondingly, the c.m. momentum of the incoming particles gets changed :  $q(\sqrt{s^*}, m_N^*, m_N^*) \leq q(\sqrt{s}, m_N, m_N)$ .

Replacing only the vacuum cross sections by the in-medium ones in BUU would, however, not correspond to a consistent description of the resonance production/absorption rates because

$$w_{12 \rightarrow 34} \propto v_{12}^* \sigma_{12 \rightarrow 34}^{med} \quad (69)$$

where  $w_{12 \rightarrow 34}$  is the transition probability per unit time.

$$v_{12}^* = \frac{\sqrt{s^*}}{\varepsilon_1^* \varepsilon_2^*} q(\sqrt{s^*}, m_1^*, m_2^*) \quad (70)$$

is the relative velocity and  $\varepsilon_i^* = \sqrt{q^2 + (m_i^*)^2}$ ,  $i = 1, 2$  are the c.m. energies of colliding particles 1 and 2. Due to the difference between the mean fields in BUU and in the RMF model, the relative velocities of colliding particles are, generally, different in both models too. Therefore, in order to obtain the rates corresponding to the RMF model, we have multiplied the cross sections calculated above by the factor  $v_{12}^* / v_{12}^{BUU}$ , where  $v_{12}^{BUU}$  is the relative velocity of the colliding particles as given by BUU.

The BUU results have been obtained by applying the soft momentum dependent mean field (SM,  $K = 220$  MeV, see Refs. [44, 46] for details) in the Hamiltonian propagation of baryons. Fig. 13 shows the time dependence of the sum of the pion and  $\Delta$  multiplicities in a central collision of Au+Au at 1.06 A GeV. At  $t = 40$  fm/c practically all the  $\Delta$ 's have already decayed, so that the final pion multiplicity can be determined from Fig. 13. A standard calculation without any in-medium effects in the cross sections ends up with 68 pions, which is much more than the experimental value of  $41 \pm 7$  [12]. Using the medium modified cross sections reduces the pion multiplicity. A bigger reduction corresponds to a steeper dropping effective mass with the density (c.f. Fig. 5). Thus, the smallest pion multiplicity of  $\sim 34$  is obtained within the NL1-Set2 combination. It is interesting that the combinations NL1-Set1 and NL2-Set2 produce nearly equal pion numbers : 45 and 43, respectively. This is explained by the fact, that the maximum central density reached in central Au+Au collisions at 1 A GeV is about  $2.4\rho_0$ , while the cross sections given by the NL1-Set1 and NL2-Set2 combinations are similar at  $\rho < 3\rho_0$  (see Fig. 10). In all calculations below we will always use the Set2 of the OPEM parameters, thus, we will drop for brevity the label “Set2”.

Fig. 14 shows the average total pion multiplicity  $\langle n_\pi \rangle$  divided by the average participant number  $\langle A_{part} \rangle$  as a function of the total mass number  $A_{sys}$  of colliding nuclei in comparison to the data [12]. The systems Ca+Ca, Ru+Ru and Au+Au were studied at the beam energies of 400, 1000 and 1500 A MeV. Following [12], we have fitted the total pion multiplicity as a function of the participant number  $A_{part}$  by a straight line in the range  $0.15 < A_{part}/A_{sys} < 0.85$ . The participant number  $A_{part}$  has been extracted from the geometrical overlap of colliding nuclei for a given impact parameter taking into account smooth

density profiles as described in [12].

First, we notice that there is no a single set of parameters which is able to describe all data points in Fig. 14 simultaneously. The standard calculation agrees with the data at 400 A MeV, but it clearly overpredicts the experiment at 1000 A MeV and, for heavy systems, also at 1500 A MeV.

The NL1 parameterization works for the Au+Au system at 1000 and 1500 A MeV, however, it is below the data at 400 A MeV. Furthermore, NL1 is unable to describe the experimental slopes at 1000 and 1500 A MeV.

RHA is in the best agreement with data at 400 A MeV. Surprisingly, for the Au+Au system at 400 A MeV RHA gives more pions than the standard calculation. This, probably, can be explained by the reduced reabsorption of  $\Delta$ 's in RHA due to the in-medium reduced cross section  $\Delta N \rightarrow NN$ . RHA is also rather close to the experiment at 1000 A MeV, while at 1500 A MeV the system mass dependence is too flat within RHA.

The best overall description of pion multiplicities seems to be reached within the NL2 parameterization. More precise data, in particular, at the lowest energy are needed for definite conclusions, however.

Fig. 15 shows the ratio of the average  $\pi^-$  and  $\pi^+$  multiplicities vs the total mass number of a system for Ca+Ca, Ru+Ru and Au+Au at 400, 1000 and 1500 A MeV in comparison to the data [12]. The calculated ratio  $\langle n_{\pi^-} \rangle / \langle n_{\pi^+} \rangle$  practically does not depend on the in-medium modifications of the cross sections, since these modifications do not change the ratios between the cross sections for various isospin channels. For Ca+Ca and Ru+Ru all the calculations agree with the data, while for the Au+Au system there is a systematic tendency to produce about 10 % too many  $\pi^-$ 's in our calculations. Probably, the  $\langle n_{\pi^-} \rangle / \langle n_{\pi^+} \rangle$  ratio would be described better if to take into account the isospin dependence of the in-medium part of the nucleon propagator (40).

Fig. 16 shows the inclusive transverse momentum spectra of pions at midrapidity for the Au+Au system at 1.06 A GeV. The standard calculation (dotted line) overpredicts the data at  $p_t > 150$  MeV/c. NL1 (dashed line) leads to a good description at  $p_t > 200$  MeV/c, but it underpredicts the experiment at low  $p_t$ . Almost the same result has been obtained earlier in [13] using the phenomenological density dependent quenching factor for the  $NN \leftrightarrow N\Delta$  cross sections. A better overall description is reached within the NL2 parameterization (dash-dotted line), however the yields of  $\pi^-$ 's and  $\pi^0$ 's are still underpredicted in the region

of small transverse momenta. This is improved by taking into account the pion off-shellness in BUU [47] (solid line), which enhances the soft pion yield keeping the total pion number practically unchanged.

In order to see how the density modified cross sections work in the case of light colliding nuclei we selected the TAPS data on  $\pi^0$  production from collisions of C+C at 0.8, 1.0 and 2.0 A GeV [48]. Fig. 17 shows the impact parameter averaged  $\pi^0$  multiplicity  $\langle M \rangle_{\Delta y}$  in a narrow rapidity interval near  $y = 0$ . Standard calculation is in the best agreement with the data for  $\langle M \rangle_{\Delta y}$ , while the NL1 and NL2 calculations are below the data for the beam energies of 0.8 and 1 A GeV.

Finally, Fig. 18 shows transverse mass spectra of  $\pi^0$ 's at midrapidity for the C+C collisions at 0.8, 1 and 2 A GeV. The standard calculation provides a quite good description of the data [48]. In-medium modifications of the cross sections do not destroy a good description at 2 A GeV and also improve agreement with experiment for large transverse masses for 0.8 and 1 A GeV, but tend to underpredict the data at small  $m_t$  for 0.8 and 1 A GeV.

#### IV. SUMMARY

In this work we have calculated the in-medium  $NN \rightarrow N\Delta(1232)$  cross section within the OPEM taking into account the exchange pion collectivity, vertex corrections by the contact nuclear interactions and the effective masses of the nucleon and  $\Delta$  resonance.

- (i) We have observed that even without the effective mass modifications the cross section decreases with the nuclear matter density at high densities if one takes into account the in-medium  $\Delta$  width and includes the  $NN^{-1}$  Lindhard function in the calculations (Fig. 11).
- (ii) Inclusion of the effective mass modifications for the nucleons and  $\Delta$ 's leads to an additional strong reduction of the cross section.
- (iii) The FOPI data [12] on the total pion multiplicity from the systems Ca+Ca, Ru+Ru and Au+Au at 0.400, 1.000 and 1.500 A GeV seem to require a dropping effective mass with the baryon density (NL2 version of the RMF model) in combination with the universal value of 0.6 for all the Landau-Migdal parameters in the spin-isospin channel. We note that this still depends somewhat on the size of the  $\Delta$ -spreading width used (80 MeV  $\rho/\rho_0$  [34, 35]). More precise data on the total pion multiplicity are needed in order to better select the model for the density dependence of the Dirac effective masses of the baryons.

The effect of the medium modifications of the  $NN \leftrightarrow N\Delta$  cross sections on the pion multiplicity depends also on the assumption about other channels of the pion production/absorption in NN collisions, most importantly, on the  $s$ -wave direct channel  $NN \leftrightarrow NN\pi$ . Including the effective mass modifications in the  $NN \leftrightarrow N\Delta$  channel *only*, does not lead to strong enough reduction of the observed pion multiplicity, since then more pions are produced in the  $s$ -wave channel. The in-medium modifications of the higher resonance cross sections do not influence the pion production at 1-2 A GeV collision energy sensitively : other particles like  $\eta$  and  $\rho$  mesons are, probably, more sensitive to higher resonance in-medium modifications.

The calculations with the in-medium modified cross sections slightly underpredict the low transverse mass  $\pi^0$  yield at midrapidity for C+C collisions at 0.8 and 1.0 A GeV (Fig. 18). This implies, that with decreasing mass number of the colliding system the in-medium corrections disappear faster than in our model. The reason could be a strong nonequilibrium momentum distribution at the beginning of collision: instead of one Fermi sphere there are two nonoverlapping Fermi spheres, which is not taken into account in our calculation of the effective mass. Indeed, the nonequilibrium momentum distribution reduces the scalar density, and, therefore, increases the effective mass. This effect is expected to be stronger for lighter systems, since smaller baryon density is reached in this case.

Another open problem is the general tendency of the transport models to overpredict pion multiplicity in heavy colliding systems at AGS energies (c.f. Ref. [11]). This problem can not be solved by just density modifications of the resonance production/absorption cross sections, since most pions are produced by the string mechanism here. In-medium modifications of the FRITIOF model, thus, could help to solve this problem.

### Acknowledgments

Numerous stimulating discussions with M. Post and Dr. L. Alvarez-Ruso are gratefully acknowledged. The authors are grateful to Markus Post for the reading of the manuscript before publication, critical comments and suggestions and to Luis Alvarez-Ruso for pointing out Ref. [28] which has influenced our results.

## APPENDIX A: CALCULATION OF $\overline{|T_a^{med}|^2}$ FOR THE PROCESS $pp \rightarrow n\Delta^{++}$

For the calculation of  $\overline{|T_a^{med}|^2}$  it is convenient to introduce the renormalized coupling constants

$$\tilde{f}_\Delta(k) \equiv \det^{-1}(\hat{A}(k))[1 + (g'_{NN} - g'_{N\Delta})\chi_N(k)]f_\Delta(k^2), \quad (A1)$$

$$\tilde{f}(k) \equiv \det^{-1}(\hat{A}(k))[1 + (g'_{\Delta\Delta} - g'_{N\Delta})\chi_\Delta(k)]f(k^2) \quad (A2)$$

and the renormalized Landau-Migdal parameter

$$\tilde{g}(k) \equiv \frac{\det(\hat{A}(k))g'_{N\Delta}}{[1 + (g'_{NN} - g'_{N\Delta})\chi_N(k)][1 + (g'_{\Delta\Delta} - g'_{N\Delta})\chi_\Delta(k)]}. \quad (A3)$$

In terms of  $\tilde{f}_\Delta(k)$ ,  $\tilde{f}(k)$  and  $\tilde{g}(k)$  the renormalized vertex operators and the renormalized contact interaction have the same form as the vacuum ones :

$$\tilde{\Gamma}_j^{abs}(k) = -\frac{\tilde{f}_\Delta(k)}{m_\pi}(\mathbf{S} \cdot \mathbf{k})T_j, \quad (A4)$$

$$\tilde{\Gamma}_j^{dec}(k) = \frac{\tilde{f}(k)}{m_\pi}(\boldsymbol{\sigma} \cdot \mathbf{k})\tau_j, \quad (A5)$$

$$\tilde{V}_{4,3;2,1}(k) = \frac{\tilde{f}_\Delta(k)\tilde{f}(k)}{m_\pi^2}\tilde{g}(k)[\chi_\Delta^\dagger(4)S_\alpha \mathbf{T}\chi(2)][\chi^\dagger(3)\sigma_\alpha \boldsymbol{\tau}\chi(1)]. \quad (A6)$$

Notice, that  $\tilde{f}_\Delta(k)$ ,  $\tilde{f}(k)$  and  $\tilde{g}(k)$  are complex-valued quantities. Substituting (A4),(A5) and (A6) into (10) on the place of corresponding vacuum quantities and also replacing  $(\mathbf{S} \cdot \mathbf{k}) \rightarrow (\mathbf{S} \cdot \mathbf{k}_4)$  (see Eq.(21)) in Eq.(A4) one can get after some algebra :

$$\begin{aligned} \overline{|T_a^{med}|^2} &= \frac{1}{4} \sum_{\lambda_1, \lambda_2, \lambda_3, \lambda_{\Delta 4}} |T_a^{med}|^2 = \frac{4}{3} \frac{|\tilde{f}_\Delta(k)|^2 |\tilde{f}(k)|^2}{m_\pi^4} \\ &\times \left[ \mathbf{k}_4^2 \mathbf{k}^2 |D(k)|^2 + (\tilde{g}^*(k)D(k) + \tilde{g}(k)D^*(k))(\mathbf{k}_4 \cdot \mathbf{k}) + 3|\tilde{g}(k)|^2 \right] \left( -\frac{t}{\mathbf{k}^2} \right), \quad (A7) \end{aligned}$$

where the term  $-t/\mathbf{k}^2$  is introduced in order to restore the Lorentz invariance, as discussed in Sect. II. The exchange term  $\overline{|T_b^{med}|^2}$  is given by Eq.(A7) with replacements  $k \rightarrow k'$ ,  $t \rightarrow u$  and  $\mathbf{k}_4 \rightarrow \mathbf{k}'_4$  (see Eq.(22)).

For the spin-averaged interference term we get :

$$\begin{aligned} \frac{1}{4} \sum_{\lambda_1, \lambda_2, \lambda_3, \lambda_{\Delta 4}} [T_a^{med}(T_b^{med})^* + (T_a^{med})^*T_b^{med}] &= -\frac{\tilde{f}_\Delta^*(k')\tilde{f}^*(k')\tilde{f}_\Delta(k)\tilde{f}(k)}{m_\pi^4} \\ &\times \left\{ \frac{1}{3} [2(\mathbf{k}'_4 \cdot \mathbf{k}_4)(\mathbf{k}' \cdot \mathbf{k}) + (\mathbf{k}_4 \cdot \mathbf{k})(\mathbf{k}'_4 \cdot \mathbf{k}') - (\mathbf{k}_4 \cdot \mathbf{k}')(\mathbf{k}'_4 \cdot \mathbf{k})]D^*(k')D(k) \right. \\ &+ \left. \frac{4}{3}(\mathbf{k}'_4 \cdot \mathbf{k}')D^*(k')\tilde{g}(k) + \frac{4}{3}(\mathbf{k}_4 \cdot \mathbf{k})D(k)\tilde{g}^*(k') + 4\tilde{g}^*(k')\tilde{g}(k) \right\} \frac{(tu)^{1/2}}{(\mathbf{k}^2 \mathbf{k}'^2)^{1/2}} + c.c. . \quad (A8) \end{aligned}$$

## APPENDIX B: IN-MEDIUM CROSS SECTIONS FOR THE INVERSE PROCESSES

We use below the detailed balance principle, i.e. the equality of the matrix elements of the direct and inverse processes, in order to get the cross sections for the reactions  $N\Delta \rightarrow NN$ ,  $NR \rightarrow NN$ ,  $\Delta\Delta \rightarrow NN$  and the pion  $s$ -wave absorption rate by two-nucleon pairs  $\pi NN \rightarrow NN$ .

The in-medium differential cross section for the process  $N\Delta \rightarrow NN$  is given by the expression (c.f. Eq.(32)) :

$$\frac{d\sigma_{N_3\Delta_4 \rightarrow N_1N_2}^{med}(\sqrt{s^*})}{d\Omega} = \frac{(2m_N^*)^3 2M_\Delta^*}{64\pi^2 s^*} \frac{2}{2J_\Delta + 1} \frac{\overline{|T^{med}|^2} q(\sqrt{s^*}, m_N^*, m_N^*)}{q(\sqrt{s^*}, M_\Delta^*, m_N^*)} S_{12} , \quad (B1)$$

where  $\overline{|T^{med}|^2}$  is calculated in Appendix A (Eqs. (A7),(A8)).  $J_\Delta = 3/2$  is the spin of the  $\Delta$ -resonance. For the process  $NR \rightarrow NN$ , where  $R$  means one of the higher resonances, one should simply replace in Eq.(B1) “ $\Delta$ ” by “ $R$ ” : now  $M_R^*$  and  $J_R$  are the effective mass and spin of the resonance  $R$ , respectively.  $\overline{|T^{med}|^2}$  is now a constant depending only on the isospin channel.

The in-medium cross section of the reaction  $\Delta\Delta \rightarrow NN$  reads as follows (c.f. Eq.(65)) :

$$\begin{aligned} \sigma_{\Delta_3\Delta_4 \rightarrow N_1N_2}^{med}(\sqrt{s^*}) &= \frac{(2m_N^*)^2 (2m_\Delta^*)^2}{16\pi s^*} \frac{4}{(2J_\Delta + 1)^2} \overline{|T_{N_1N_2 \rightarrow \Delta_3\Delta_4}|^2} \\ &\times \frac{q(\sqrt{s^*}, m_N^*, m_N^*)}{q(\sqrt{s^*}, M_3^*, M_4^*)} S_{12} . \end{aligned} \quad (B2)$$

The pion  $s$ -wave absorption rate by the two-nucleon pairs is :

$$\begin{aligned} \Sigma_\pi^{med} > (k) &= \frac{1}{2k_0} \sum_{1,2} \int \frac{gd^3p_1}{(2\pi)^3 2\varepsilon_1^*} n_1 \frac{gd^3p_2}{(2\pi)^3 2\varepsilon_2^*} n_2 \frac{gd^3p_3}{(2\pi)^3 2\varepsilon_3^*} (1 - n_3) \frac{gd^3p_4}{(2\pi)^3 2\varepsilon_4^*} (1 - n_4) \\ &\times (2\pi)^4 \delta^{(4)}(k + p_1^* + p_2^* - p_3^* - p_4^*) S_{12} S_{34} (2m_N^*)^4 \overline{|T_{N_3N_4 \rightarrow N_1N_2\pi}|^2}(\sqrt{s}) , \end{aligned} \quad (B3)$$

where  $g = 2$  is the nucleon spin degeneracy factor,  $n_i \equiv n(\mathbf{p}_i)$ , ( $i = 1, 2, 3, 4$ ) are the nucleon occupation numbers. The sum in Eq.(B3) is taken over the isospin projections of the incoming nucleons 1 and 2. The vacuum matrix element squared

$$\overline{|T_{N_3N_4 \rightarrow N_1N_2\pi}|^2}(\sqrt{s}) = \frac{(2\pi)^3 64q(\sqrt{s}, m_N, m_N)s^{3/2} \sigma_{N_3N_4 \rightarrow N_1N_2\pi}^{vac}(\sqrt{s})}{(2m_N)^4 S_{12} \int d(m_{12})^2 d(m_{2\pi})^2} \quad (B4)$$

depends on the vacuum c.m. energy and on the particle isospins. The integral (B3) is performed by the Monte-Carlo method as described in Ref. [44].

---

[1] G.F. Bertsch and S. Das Gupta, Phys. Rep. **160**, 189 (1988).

[2] W. Cassing, V. Metag, U. Mosel, and K. Niita, Phys. Rep. **188**, 363 (1990).

[3] U. Mosel, Annu. Rev. Nucl. Part. Sci., **41**, 29 (1991).

[4] W. Ehehalt, W. Cassing, A. Engel, U. Mosel, and Gy. Wolf, Phys. Rev. C **47**, R2467 (1993).

[5] S.A. Bass, C. Hartnack, H. Stoecker, W. Greiner, Phys. Rev. C **51**, 3343 (1995).

[6] C.M. Ko and G.Q. Li, J. Phys. **G 22**, 1673 (1996).

[7] S. Teis, W. Cassing, M. Effenberger, A. Hombach, U. Mosel and Gy. Wolf, Z. Phys. A **356**, 421 (1997);  
S. Teis, W. Cassing, M. Effenberger, A. Hombach, U. Mosel and Gy. Wolf, Z. Phys. A **359**, 297 (1997).

[8] J. Helgesson and J. Randrup, Phys. Lett. B **411**, 1 (1997).

[9] V.S. Uma Maheswari, C. Fuchs, Amand Faessler, L. Sehn, D.S. Kosov, Z. Wang, Nucl. Phys. A **628**, 669 (1998).

[10] W. Cassing and E.L. Bratkovskaya, Phys. Rep. **308**, 65 (1999).

[11] H. Weber, E.L. Bratkovskaya, W. Cassing, H. Stöcker, Phys. Rev. C **67**, 014904 (2003).

[12] D. Pelte et al., Z. Phys. A **357**, 215 (1997); M.R. Stockmeier et al., GSI Scientific Report 2001, p. 35.

[13] A.B. Larionov, W. Cassing, S. Leupold, U. Mosel, Nucl. Phys. A **696**, 747 (2001).

[14] B. ter Haar and R. Malfliet, Phys. Rev. C **36**, 1611 (1987).

[15] G.F. Bertsch, G.E. Brown, V. Koch and B.-A. Li, Nucl. Phys. A **490**, 745 (1988).

[16] J.Q. Wu and C.M. Ko, Nucl. Phys. A **499**, 810 (1989).

[17] J. Helgesson and J. Randrup, Ann. Phys. (N.Y.) **244**, 12 (1995).

[18] T. Ericson and W. Weise, Pions and Nuclei, Clarendon Press, Oxford, 1988.

[19] V. Dmitriev, O. Sushkov and C. Gaarde, Nucl. Phys. A **459**, 503 (1986).

[20] G.E. Brown and W. Weise, Phys. Rep. **22**, 279 (1975).

[21] J. Meyer-Ter-Vehn, Phys. Rep. **74**, 323 (1981).

[22] A.B. Migdal, E.E. Saperstein, M.A. Troitsky and D.N. Voskresensky, Phys. Rep. **192**, 179 (1990).

[23] E. Oset and M. Rho, Phys. Rev. Lett. **42**, 47 (1979).

- [24] B. Körfgen, P. Oltmanns, F. Osterfeld and T. Udagawa, Phys. Rev. C **55**, 1819 (1997).
- [25] P. Arve and J. Helgesson, Nucl. Phys. A **572**, 600 (1994).
- [26] J.D. Bjorken and S.D. Drell, *Relativistic quantum mechanics*, McGraw-Hill, New York, 1965.
- [27] M. Effenberger, E.L. Bratkovskaya, and U. Mosel, Phys. Rev. C **60**, 44614 (1999).
- [28] P. Fernández de Córdoba, E. Oset, M.J. Vicente-Vacas, Yu. Ratis, J. Nieves, B. López-Alvaredo, F. Gareev, Nucl. Phys. A **586**, 586 (1995).
- [29] A. Baldini et al., Landolt-Börnstein, V. 12, Springer Verlag, Berlin, 1987.
- [30] D.V. Bugg et al., Phys. Rev. **133**, B1017 (1964).
- [31] K. Wehrberger, C. Bedau and F. Beck, Nucl. Phys. A **504**, 797 (1989).
- [32] S.J. Lee et al., Phys. Rev. Lett. **57**, 2916 (1986).
- [33] B.D. Serot and J.D. Walecka, Adv. Nucl. Phys. **16**, 1 (1986).
- [34] M. Hirata, J.H. Koch, F. Lenz and E.J. Moniz, Ann. Phys. (N.Y.) **120**, 205 (1979).
- [35] E. Oset and L.L. Salcedo, Nucl. Phys. A **468**, 631 (1987).
- [36] R. Rapp and J. Wambach, Nucl. Phys. A **573**, 626 (1994).
- [37] H. Kim, S. Schramm, S.H. Lee, Phys. Rev. C **56**, 1582 (1997).
- [38] A.L. Fetter and J.D. Walecka, *Quantum theory of many-particle systems*, McGraw-Hill, New York, 1971.
- [39] E. Oset and A. Palanques-Mestre, Nucl. Phys. A **359**, 289 (1981).
- [40] E. Oset, P. Fernández de Córdoba, L.L. Salcedo and R. Brockmann, Phys. Rep. **188**, 79 (1990).
- [41] L.H. Xia et al., Nucl. Phys. A **485**, 721 (1988).
- [42] G.Q. Li and R. Machleidt, Phys. Rev. C **48**, 1702 (1993);  
G.Q. Li and R. Machleidt, Phys. Rev. C **49**, 566 (1994).
- [43] C. Fuchs, A. Faessler, and M. El-Shabshiri, Phys. Rev. C **64**, 024003 (2001).
- [44] M. Effenberger, PhD thesis, Uni. Giessen, 1999,  
<http://theorie.physik.uni-giessen.de/html/dissertations.html>.
- [45] K. Hagiwara et al., Phys. Rev. D **66**, 010001 (2002).
- [46] A.B. Larionov, W. Cassing, C. Greiner, and U. Mosel, Phys. Rev. C **62**, 064611 (2000).
- [47] A.B. Larionov and U. Mosel, Phys. Rev. C **66**, 034902 (2002).
- [48] R. Averbeck et al., Z. Phys. A **359**, 65 (1997).

**Table 1.** Parameters of the medium modified OPBM

Set #	$g'_{NN}$	$g'_{N\Delta}$	$g'_{\Delta\Delta}$	$\Lambda$ , GeV
1	0.9	0.4	0.4	0.70
2	0.6	0.6	0.6	0.67

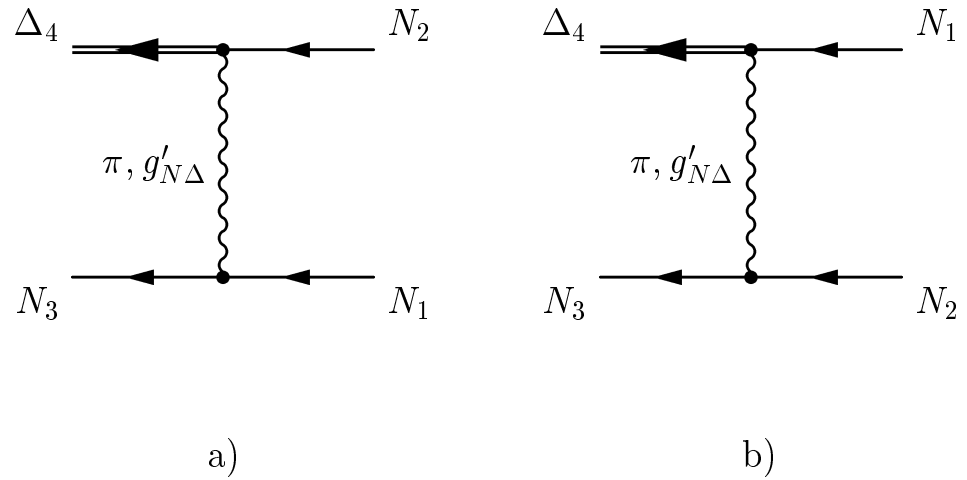


FIG. 1: Direct (a) and exchange (b) diagrams contributing to the amplitude of the process  $N_1 N_2 \rightarrow N_3 \Delta_4$ . The wiggly line denotes either  $\pi$  exchange or the contact interaction  $\propto g'_{N\Delta}$ .

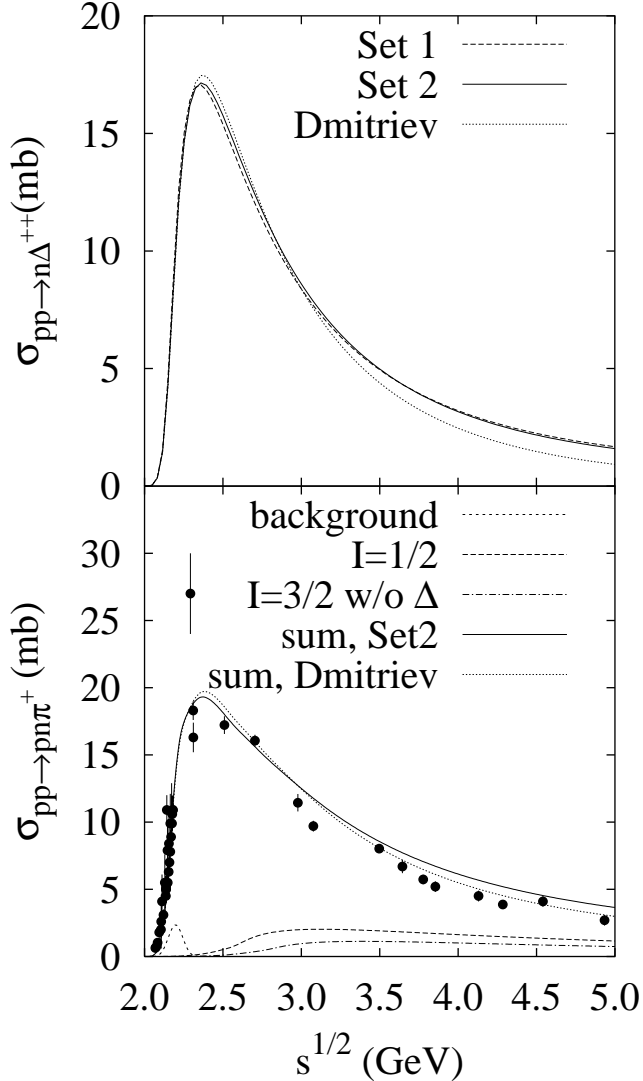


FIG. 2: Upper panel: the total cross section  $pp \rightarrow n\Delta^{++}$  in vacuum as a function of the c.m. energy  $\sqrt{s}$ . Calculations are performed using the Set 1 (dashed line) and Set 2 (solid line) of the OPEM parameters (see Table 1). Results obtained within the model of Ref. [19] are shown by dotted line. Lower panel: vacuum cross section of a single  $\pi^+$  production in  $pp$  collisions vs  $\sqrt{s}$ . Results with the  $pp \rightarrow n\Delta^{++}$  cross section calculated with the Set 2 and using the model of Ref. [19] are shown by solid and dotted lines respectively. The  $s$ -wave background, isospin 1/2 and 3/2 (excluding  $P_{33}(1232)$ ) resonance contributions [7] are shown by short-dashed, long-dashed and dash-dotted lines respectively. Solid and dotted lines show the incoherent sum of the  $pp \rightarrow n\Delta^{++}$  cross section multiplied by 10/9 and the background plus isospin 1/2 and 3/2 higher resonance contributions. The data are from Ref. [29].

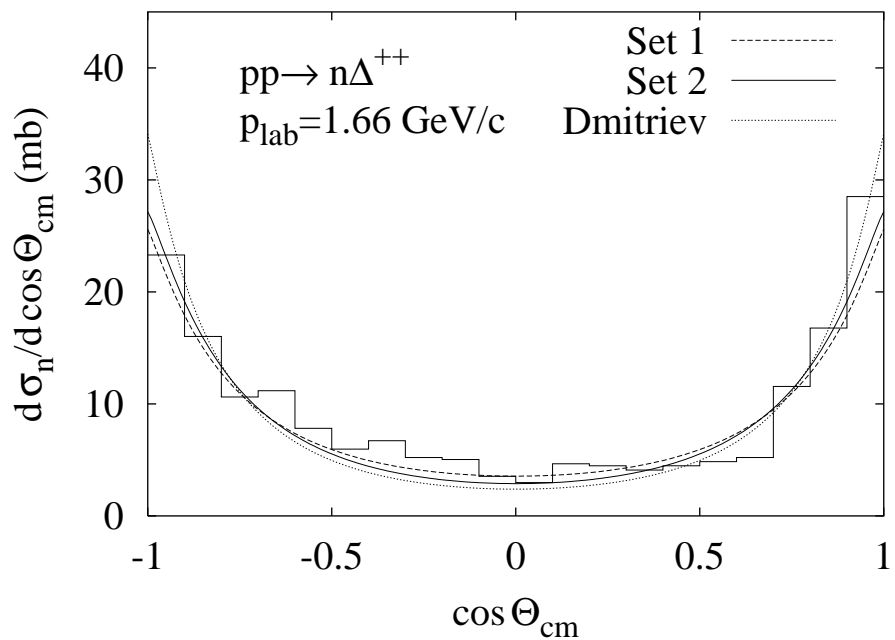


FIG. 3: Outgoing neutron c.m. polar angle distribution in the reaction  $pp \rightarrow np\pi^+$  at  $p_{lab} = 1.66$  GeV/c. In the calculations only the  $pp \rightarrow n\Delta^{++}$  channel is taken into account. The curves are labeled as in the upper panel of Fig. 2. The histogram shows the data from Ref. [30].

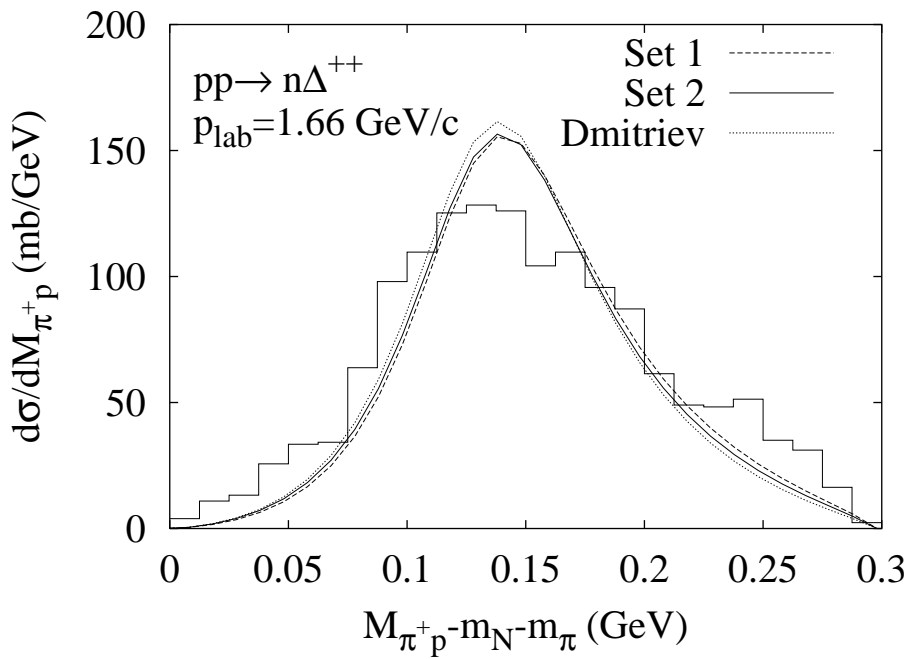


FIG. 4: Invariant mass distribution of outgoing  $\pi^+$  and proton for  $pp$  collisions at  $p_{lab} = 1.66$  GeV/c. In the calculations only the  $pp \rightarrow n\Delta^{++}$ ,  $\Delta^{++} \rightarrow \pi^+ p$  reaction channel is taken into account. The data from Ref. [30] are shown by the histogram.

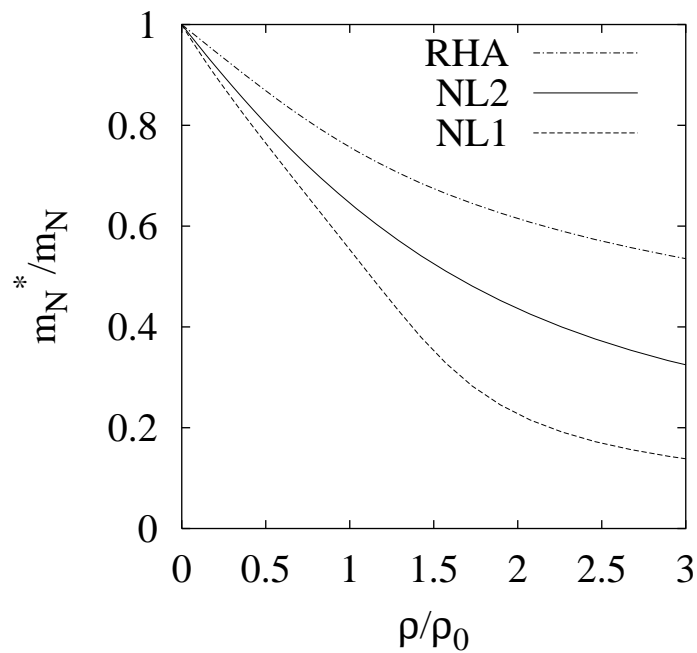


FIG. 5: Ratio of the effective nucleon mass to the vacuum nucleon mass vs the ratio of the baryon density to the nuclear saturation density. Dashed, solid and dash-dotted lines show the calculations using NL1, NL2 and RHA respectively.

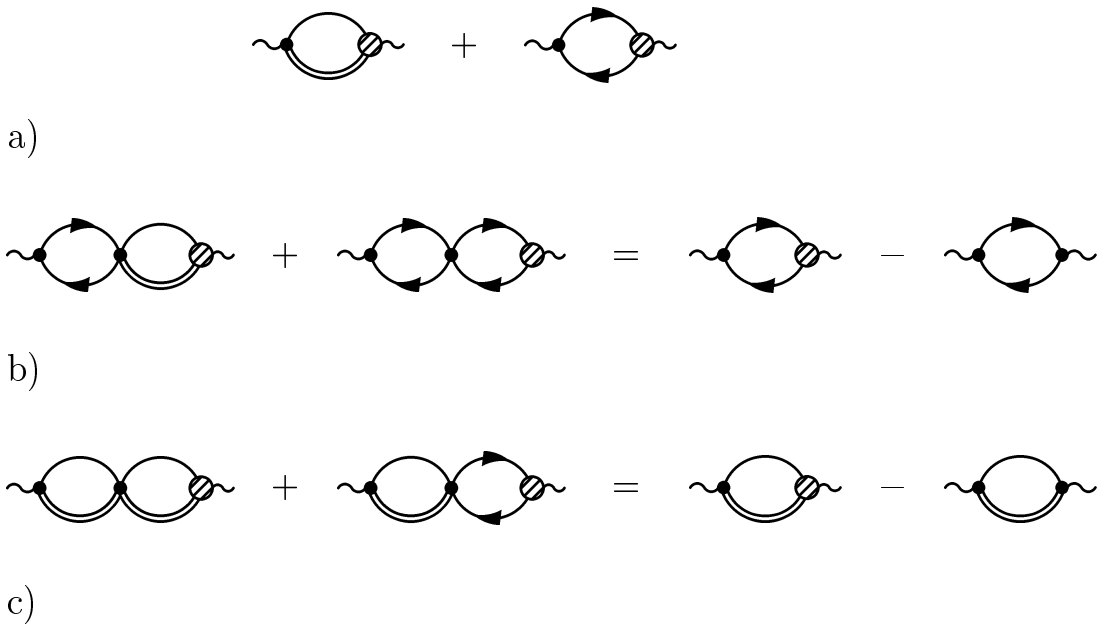
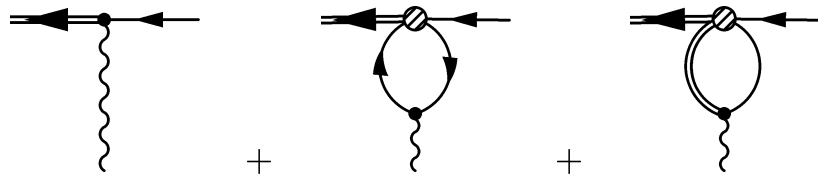
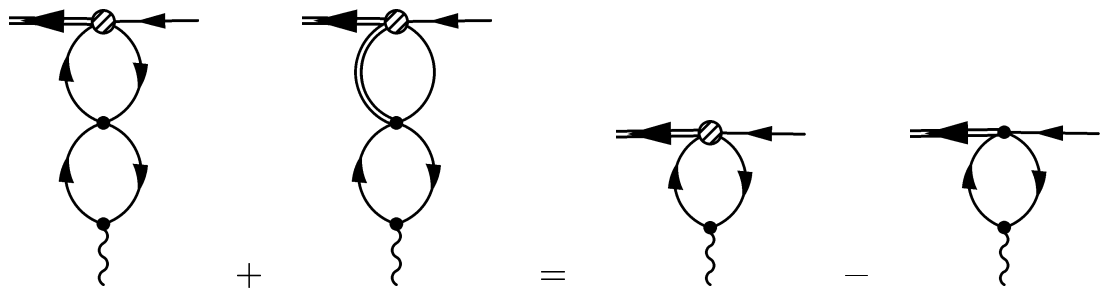


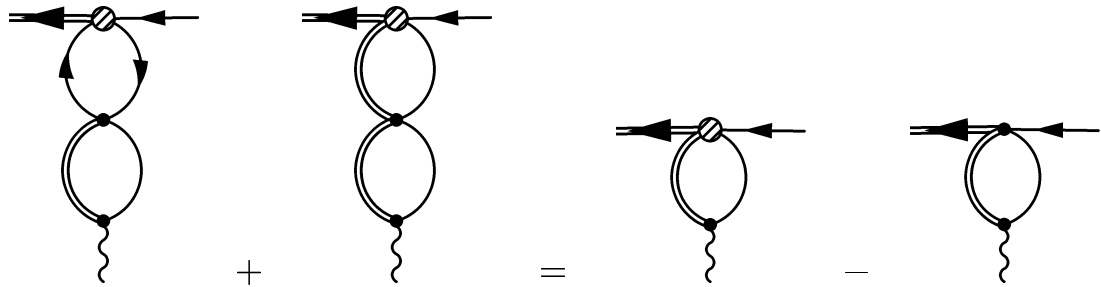
FIG. 6: (a) – Pion self-energy  $-i\Pi(k)$ . (b),(c) – The recurrence relations for the  $\Delta N^{-1}$  and  $NN^{-1}$  iterated contributions (see Eqs.(34)). Arrows are not shown on the  $\Delta N^{-1}$  loops, since each of these loops is the sum *s*- and *u*-channel graphs (with anticlockwise and clockwise directed arrows, respectively).



a)

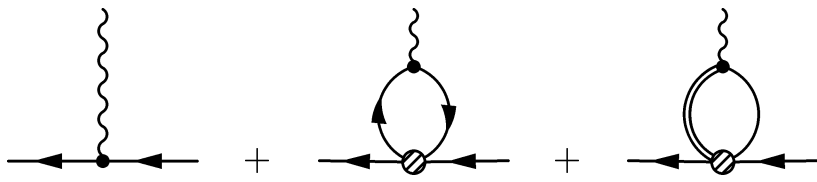


b)

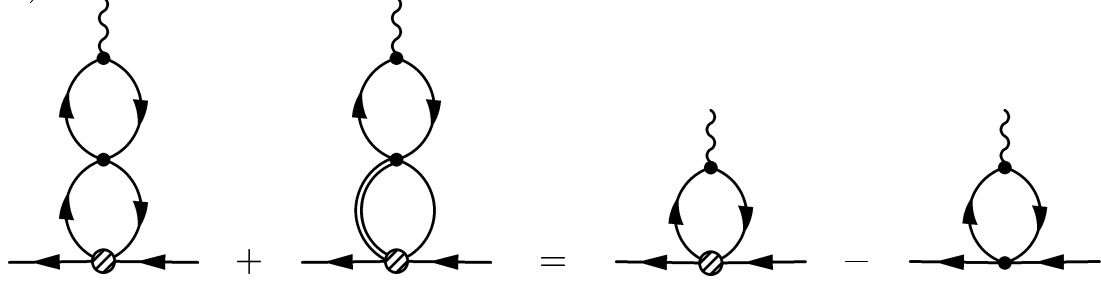


c)

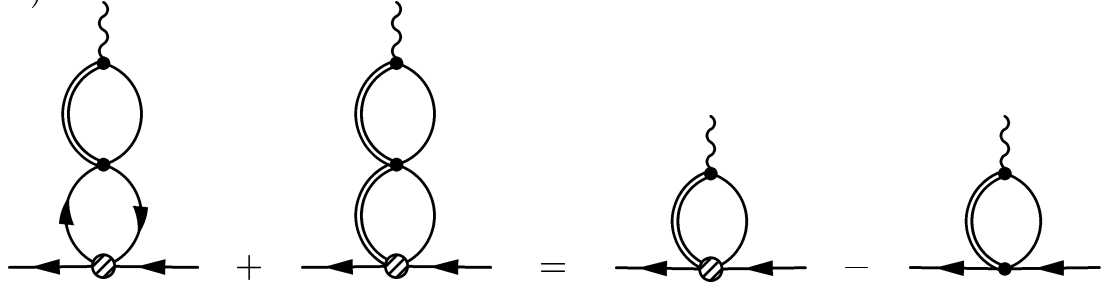
FIG. 7: (a) – Renormalized  $\pi N \Delta$  vertex operator  $\tilde{\Gamma}_j^{abs}(k)$ . (b),(c) – Recurrence relations for the  $\Delta N^{-1}$  and  $NN^{-1}$  iterated contributions to  $\tilde{\Gamma}_j^{abs}(k)$  (see Eqs.(48)).



a)



b)



c)

FIG. 8: (a) – Renormalized  $\pi NN$  vertex operator  $\tilde{\Gamma}_j^{dec}(k)$ . (b),(c) – Recurrence relations for the  $\Delta N^{-1}$  and  $NN^{-1}$  iterated contributions to  $\tilde{\Gamma}_j^{dec}(k)$  (see Eqs.(50)).

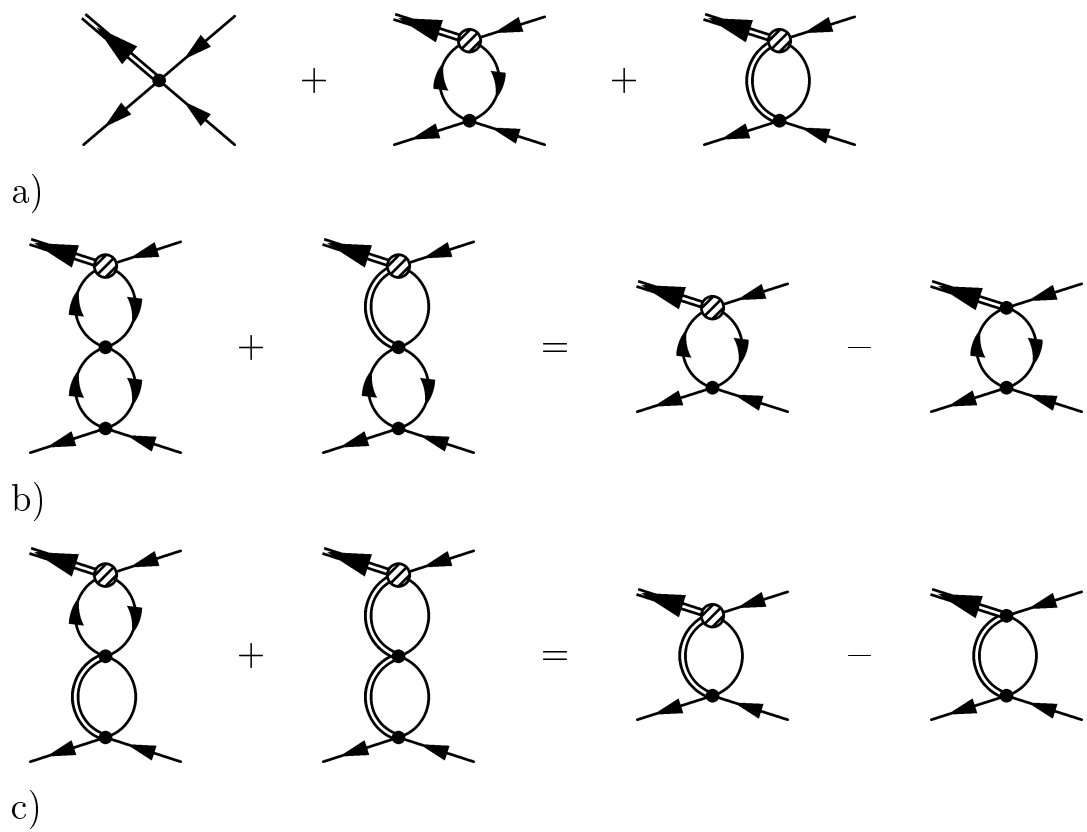


FIG. 9: (a) – Renormalized contact interaction  $-i\tilde{V}(k)$ . (b),(c) – Recurrence relations for the  $\Delta N^{-1}$  and  $NN^{-1}$  iterated contributions to  $-i\tilde{V}(k)$  (see Eqs.(52)).

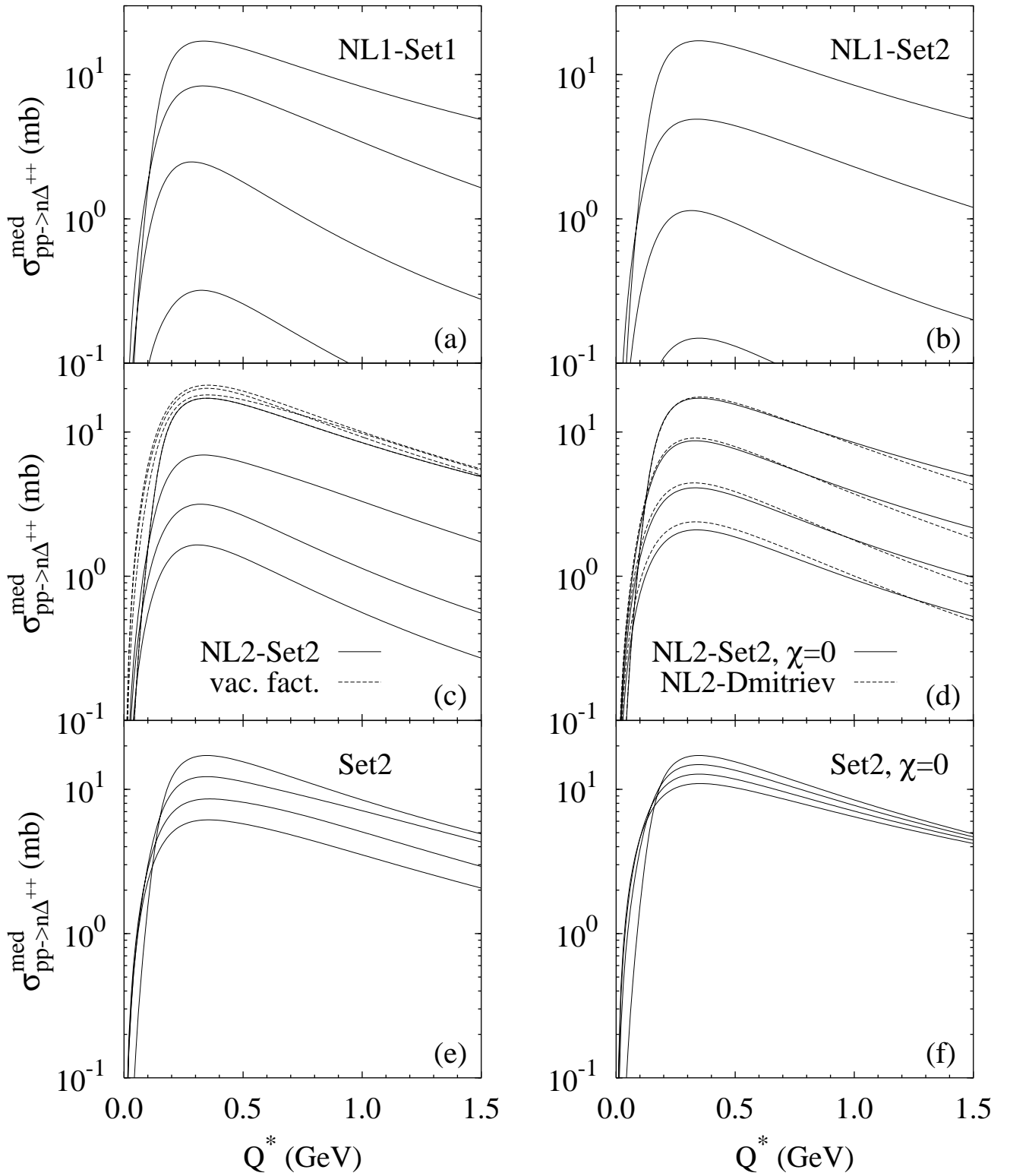


FIG. 10: In-medium  $pp \rightarrow n\Delta^{++}$  cross section as a function of the kinetic energy above the pion production threshold  $Q^*$  (see Eq.(54)) for various parameter sets (see text for details). In all cases, excepting the dashed lines in panel (c), lines from the uppermost to the lowermost correspond to the baryon densities  $\rho = 0, \rho_0, 2\rho_0$  and  $3\rho_0$ , respectively. For the dashed lines in panel (c) the density order is opposite.

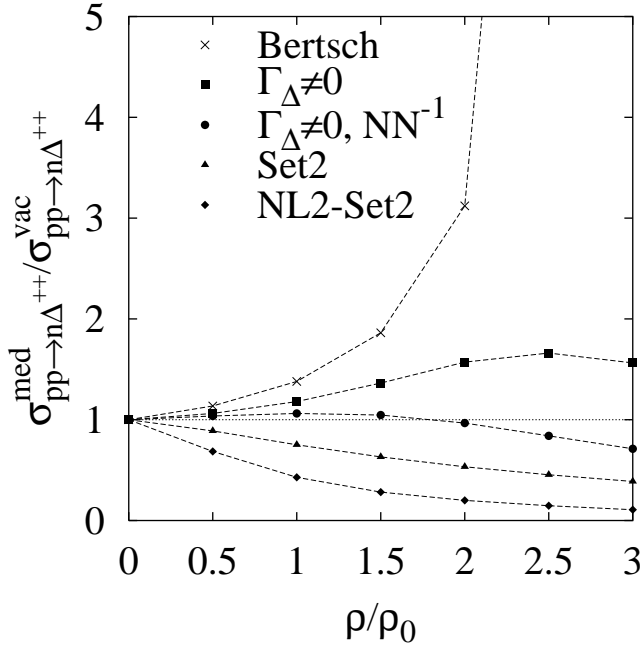


FIG. 11: Density dependence of the ratio of the in-medium and vacuum total cross sections  $pp \rightarrow n\Delta^{++}$  for  $Q^* = 0.225$  GeV (in vacuum this corresponds to the proton beam energy of 0.8 GeV). Line marked with crosses corresponds to the approximations of Ref. [15] with the parameter set B [15]. Boxes and circles show the calculations including the in-medium  $\Delta$  width without and with the  $NN^{-1}$  Lindhard function contribution respectively. Triangles and rombuses show the results for the Set2 of the OPEM parameters without and with inclusion of the effective mass, respectively.

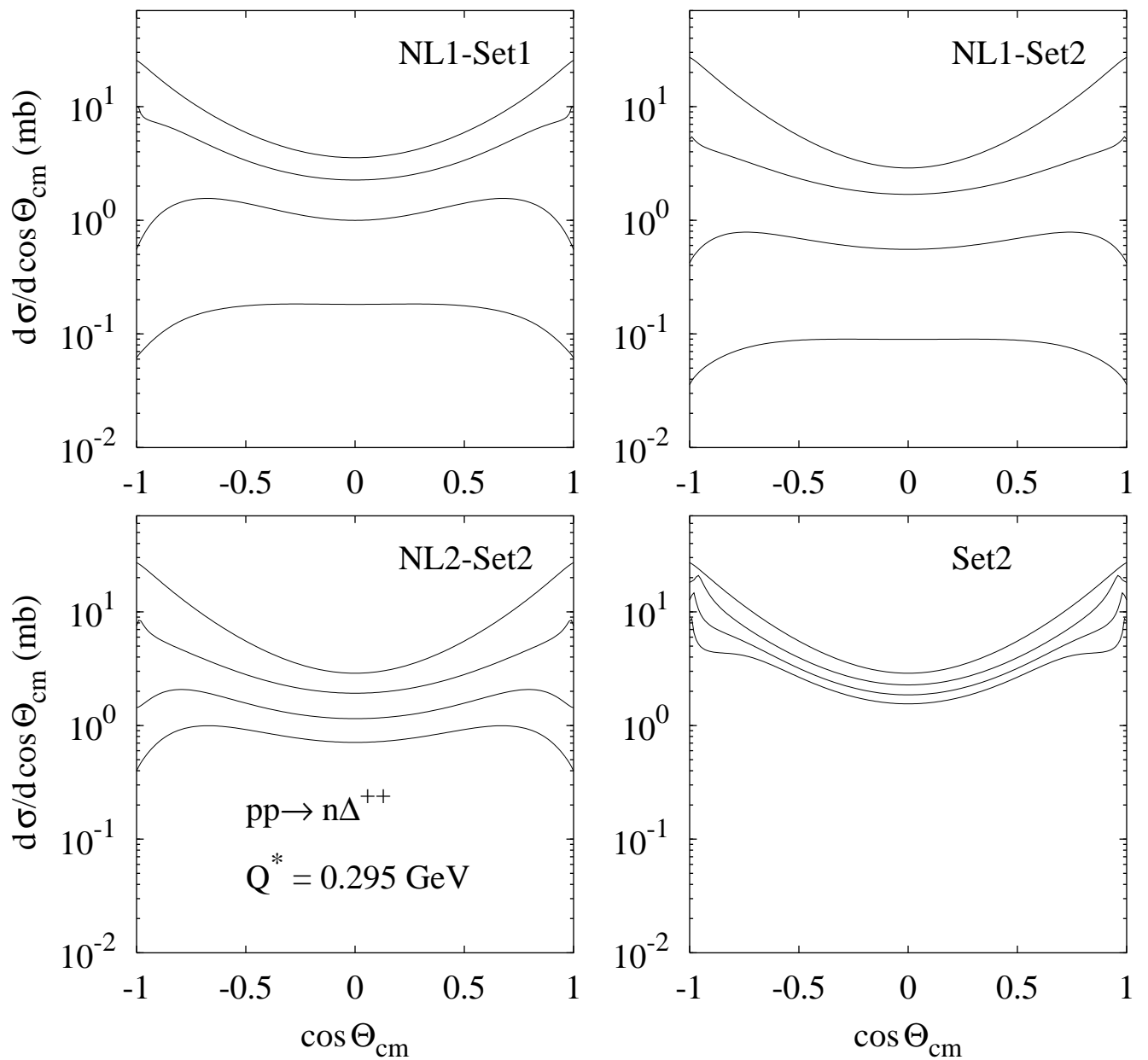


FIG. 12: Neutron c.m. polar angle dependence of the in-medium differential  $pp \rightarrow n\Delta^{++}$  cross section. The lines from the uppermost to the lowermost correspond to the baryon density  $\rho = 0, \rho_0, 2\rho_0$  and  $3\rho_0$ , respectively. Calculations are performed for  $Q^* = 0.295 \text{ GeV}$ .

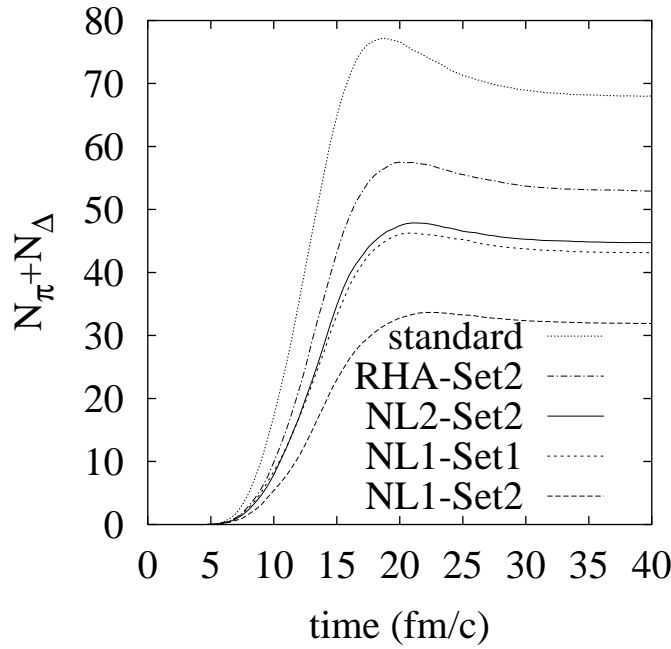


FIG. 13: Time dependence of the sum of the pion and  $\Delta$  multiplicities in the central collision of Au+Au at 1.06 AGeV. The standard BUU calculation is shown by the dotted line. The dash-dotted, solid, short-dashed and long-dashed lines show the results with the in-medium modified resonance production/absorption cross sections by using the combinations RHA-Set2, NL2-Set2, NL1-Set1 and NL1-Set2, respectively.

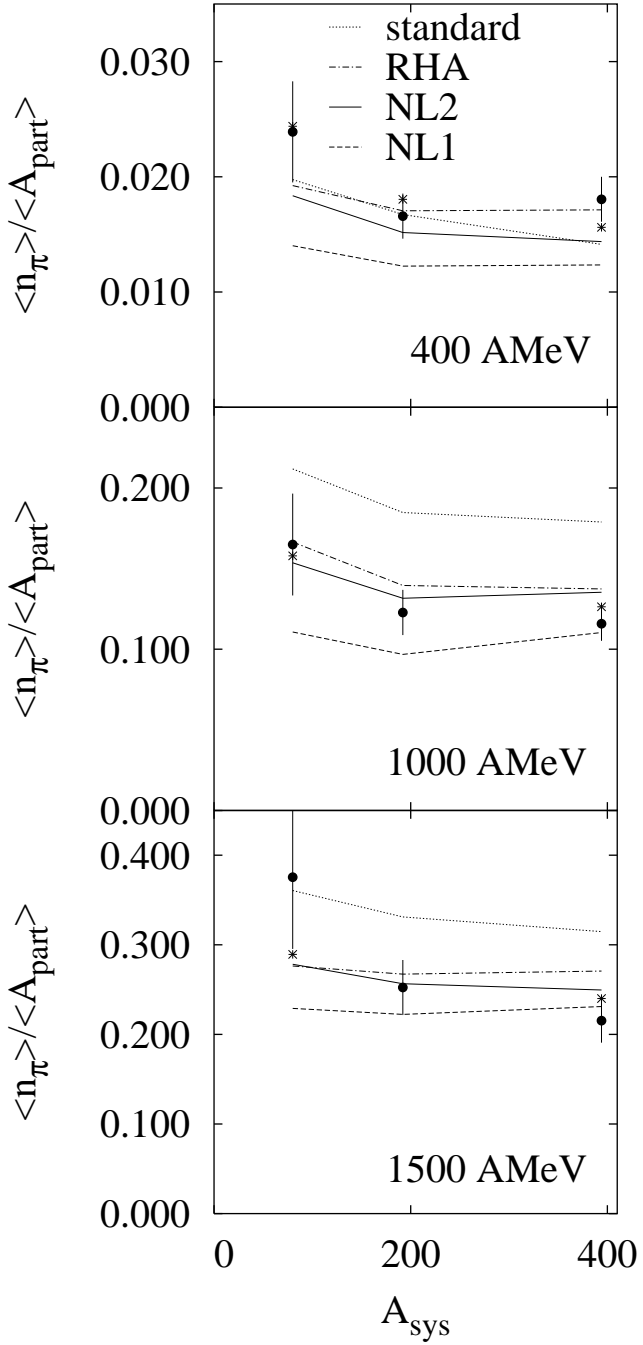


FIG. 14: Total pion yield per participating nucleon for different energies and colliding systems. Dotted, dash-dotted, solid and dashed lines correspond to the standard, RHA, NL2 and NL1 calculations, respectively. The data points are from Ref. [12]. The results of the data analysis A (B) are represented by filled circles (stars) [12].

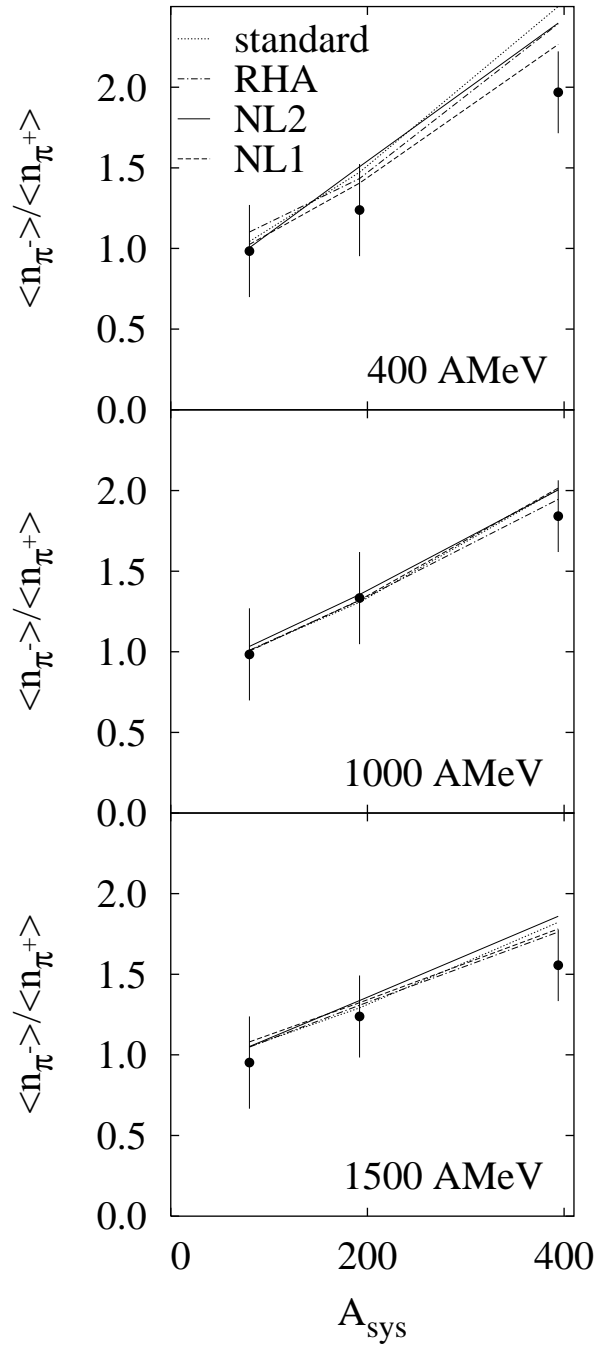


FIG. 15: Ratio of the charged pion yields for different energies and colliding systems. Various curves are denoted as in Fig. 14. The data points are from Ref. [12].

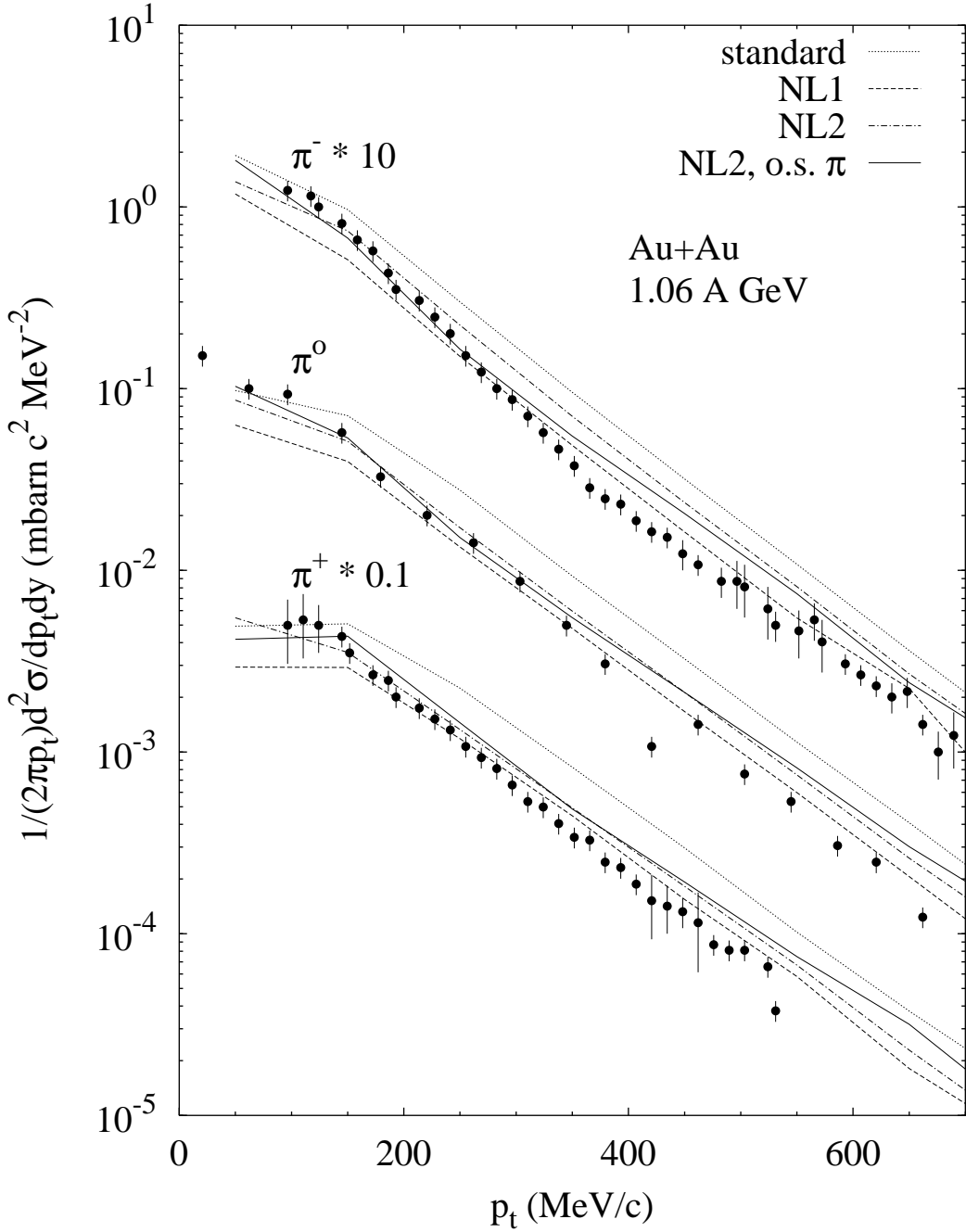


FIG. 16: Pion inclusive transverse momentum spectra at midrapidity for the reaction Au+Au at 1.06 AGeV. Dotted lines show the standard BUU calculation. Dashed and dash-dotted lines show results with in-medium modified resonance production/absorption cross sections applying the NL1 and NL2 parameterizations, respectively. Solid lines correspond to the NL2 parameterization taking into account pion off-shellness. The normalized rapidity intervals in which spectra are extracted are  $Y^{(0)} = -0.2 \div 0.2$  for  $\pi^\pm$  and  $Y^{(0)} = -0.25 \div 0.21$  for  $\pi^0$ , where  $Y^{(0)} \equiv (y/y_{proj})_{c.m.}$ . The data are from Ref. [12].

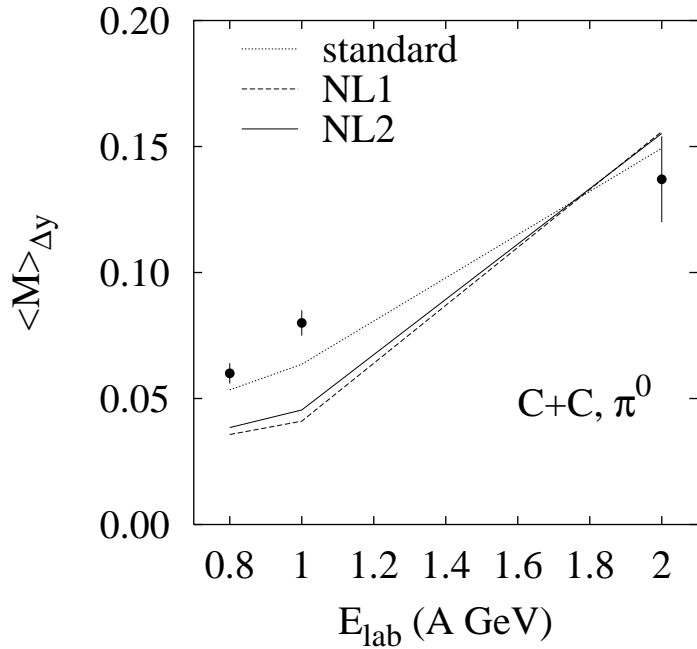


FIG. 17: The average  $\pi^0$  multiplicity in a narrow rapidity interval near midrapidity as a function of the beam energy for C+C collisions. Dotted, dashed and solid lines correspond to the standard, NL1 and NL2 calculations, respectively. The rapidity intervals are  $y = 0.42 \div 0.74$  at  $E_{lab} = 0.8$  and 1.0 A GeV, and  $y = 0.80 \div 1.08$  at  $E_{lab} = 2$  A GeV. The data are from Ref. [48].

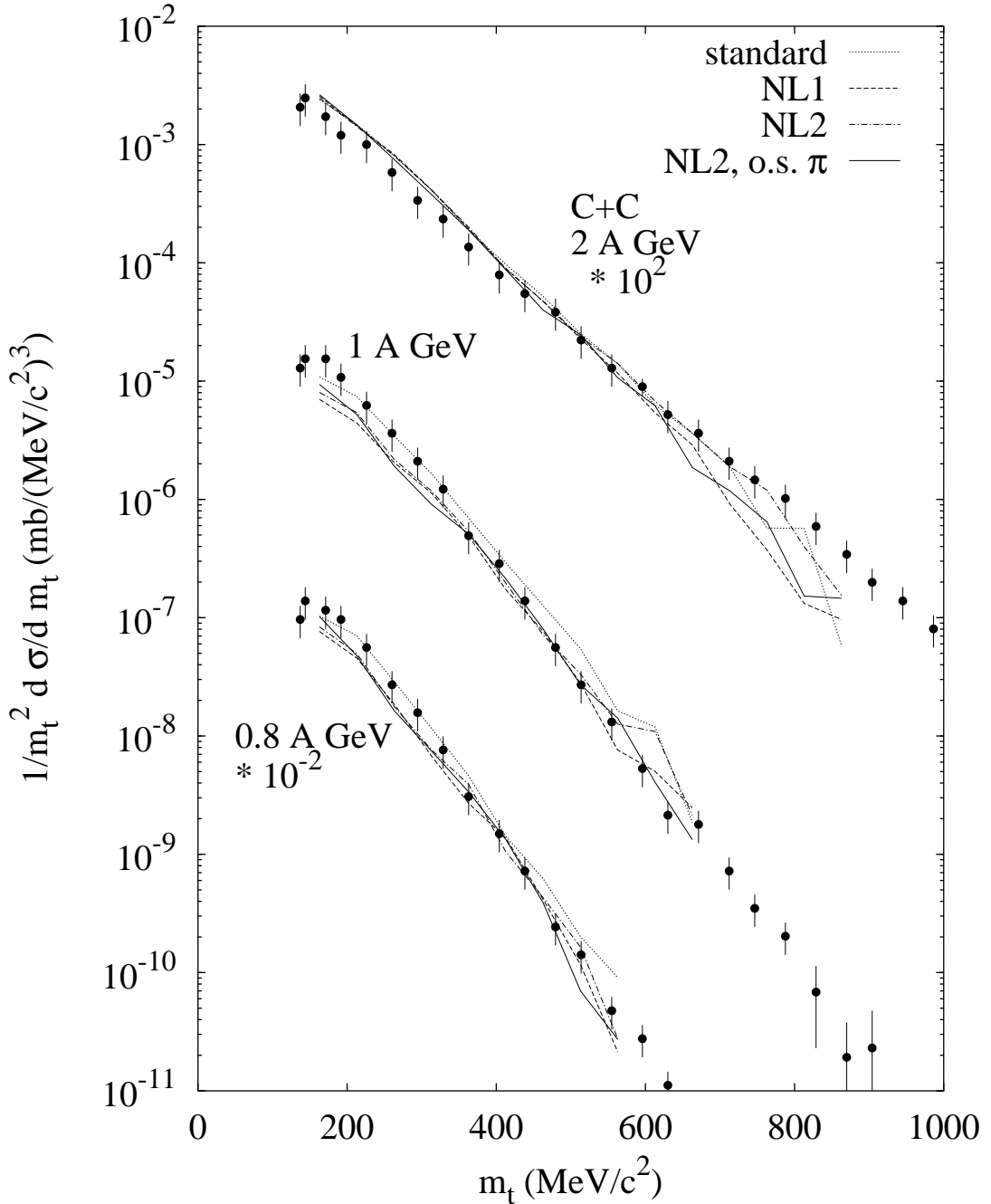


FIG. 18: Transverse mass spectra of  $\pi^0$  mesons in the narrow rapidity intervals near midrapidity (see caption to Fig. 17) for the  $^{12}\text{C} + ^{12}\text{C}$  system at 0.8, 1.0 and 2.0 A GeV. Curves are denoted as in Fig. 16. The data are from Ref. [48].